Lutein restores synaptic functionality in a *C. elegans* model for mitochondrial complex I deficiency

Silvia Maglioni [1], Alfonso Schiavi [6], Marlen Melcher [2], Vanessa Brinkmann [1], Zhongrui Luo [3], Nuno Raimundo [4], Anna Laromaine [3], Joel N Meyer [5], Felix Distelmaier [2], Natascia Ventura [1,6*]

[1] IUF-Leibniz Research Institute for Environmental Medicine, 40225 Duesseldorf, Germany

[2] Department of General Pediatrics, Neonatology and Pediatric Cardiology, University Children's Hospital, Heinrich-Heine-University Düsseldorf, Moorenstr. 5, 40225 Düsseldorf, Germany

[3] Institut de Ciència de Materials de Barcelona, ICMAB-CSIC. Campus UAB. 08193 Bellaterra, Barcelona, Spain.

[4] Institute of Cellular Biology, University Medical Center, Goettingen, Germany

[5] Nicholas School of the Environment, Duke University, Durham, NC, United States

[6] Institute for Clinical Chemistry and Laboratory Diagnostic, Medical Faculty of the Heinrich Heine University, 40225 Duesseldorf, Germany

*Corresponding author: natascia.ventura@uni-duesseldorf.de

Abstract

Complex I deficiency represents 30% of the pathogenetic causes of human mitochondrial associated diseases (HMAD), thus being the most frequent defect of mitochondrial energy metabolism. Therapeutic options for these devastating, life-threating disorders, which in most cases present with neurodevelopmental defects, do not exist, in part due to the scarcity of appropriate model systems to study them. *Caenorhabditis elegans* is a powerful, genetically tractable model organism widely used to investigate neuronal development and degeneration. Here, we generated new *C. elegans* models for HMAD, which closely recapitulated the human pathologies, and we focused on two complex I disease models associated with Leigh Syndrome, *nuo-5*/NDUFS1- and *lpd-5*/NDUFS4-depleted animals, which were exploited for a suppressor screening. We identified lutein, among a library of natural compounds, for its ability to rescue the developmental arrest and neuronal deficits in the two models. Specifically, we found that lutein exerts its beneficial activity through suppression of a synaptic defect we disclosed for the first time upon *nuo-5*/NDUFS1 depletion, thus pointing to possible novel therapeutic targets for the human disease.

Abbreviations

ACh, Acetylcholine; *C. elegans*, *Caenorhabditis elegans*; DMSO, dimethyl sulfoxide; ETC, mitochondrial electron transport chain; HCS, high-content screening; HMAD, Human Mitochondria-Associated Diseases; HTS, high-throughput screening; NGM, nematode growth medium; NDUFS1, NADH:Ubiquinone Oxidoreductase Core Subunit S1; NDUFS4, NADH:Ubiquinone Oxidoreductase Subunit S4; NMJ, neuromuscular junction; OCR, oxygen consumption rate; ROS, reactive oxygen species; RT, room temperature.

Keywords:

C. elegans; cholinergic synapses; HTS screening; Leigh syndrome; Lutein; Mitochondria diseases; neuroligin.

1 Introduction

Over the last few decades, mitochondrial dysfunction, due to mutations in either mitochondrial DNA (mtDNA) or nuclear DNA (nDNA), has been established as the cause of numerous human diseases such as Leigh syndromes, Friedreich's ataxia or Parkinson's disease [1, 2]. In these pathologies the most-affected cells are typically those highly dependent on oxidative energy metabolism such as cardiac and skeletal muscle, pancreatic beta cells and, of course, neurons. Accordingly, Human Mitochondria-Associated Diseases (HMAD) often present with signs and symptoms that include myopathy, cardiac defects, neuronal degeneration and sometimes diabetes or additional metabolic dysfunctions. Mitochondrial complex I (NADH:Ubiquinone-Oxidoreductase), the largest of the fours mitochondrial electron transport chain (ETC) complexes, consists of 44 protein subunits encoded by the nuclear and mitochondrial genomes [3, 4] and it constitutes the main entry point of electrons into the oxidative phosphorylation. Inherited genetic defects leading to human complex I deficiency are the most frequently encountered defects of the mitochondrial energy metabolism (with an incidence of about 1:8500 living births [5]) and typically cause early-onset neuro-metabolic disorders. Leigh syndrome is a

severe disorder ascribed to complex I deficiency, which leads to progressive brain damage and muscular hypotonia [6]. Unfortunately, HMAD, due to their complexity and variety, are difficult not only to diagnose but also to treat, having very often a fatal outcome, and this is in part due to the scarcity of appropriate model system to study them.

A considerable number of human disease genes have homologs in the genetically tractable model organism *Caenorhabditis elegans*, which has already yielded important insights into many of them [7-10]. *C. elegans'* small size and body transparency, short life cycle and genetic manipulability along with the absence of a requirement of ethical permits for its exploitation, make this model organism a unique and attractive tool for whole organism high-throughput (HTS) screening to search for new therapeutics [10-12]. Indeed, several works have already demonstrated the versatility of *C. elegans* in disclosing modifiers of a particular phenotype and in identifying their targets and underlying mechanisms of action; also, the number of companies that are using *C. elegans* models in the drug discovery process is growing [11]. Notably, *C. elegans* is a powerful model organism for the study of neuronal development and degeneration since 1/3 of its cells are neurons and its nervous system is well characterized both at functional and structural level. Accordingly, the nematode system is successfully used to study neuronal alterations during aging and in different age-associated disease models such as Alzheimer's or Parkinson's diseases [13, 14] and to screen for neuroprotective drugs [15, 16]. Yet, only few studies have exploited *C. elegans* to untangle the pathogenesis and identify possible new treatments for neuronal pathologies associated mitochondrial dysfunction [17-20]. Here, we developed novel *C. elegans* models for complex I deficiency, which we exploited to identify disease suppressors. We specifically followed up on our previous findings revealing a clear threshold effect in determining the opposite beneficial (e.g. lifespan extension) vs detrimental (e.g. larval arrest) phenotypes observed upon different degrees of mitochondrial stress (mild vs

severe respectively) [8, 21-23]. Of note, the discrete and very reproducible phenotypic features obtained in response to different degrees of mitochondrial dysfunction, on the one hand nicely recapitulate the progressive course of HMAD and, on the other hand, are easily quantifiable and were therefore utilized for a suppressor screening in search of new potential disease therapeutics. We identified lutein, among a library of natural compounds, for its ability to significantly suppress the arrest development and neuronal defects in two complex I-linked disease models associated with Leigh Syndrome (*nuo-5*/NDUFS1- and *lpd-5*/NDUFS4-depleted animals). Notably, we pinpoint lutein protective mechanism through suppression of a synaptic defect newly disclosed in *nuo-5*/NDUFS1-depleted animals, thus pointing to novel potential pathogenetic targets for the treatment of the human diseases and supporting the validity of the first animal model developed for this Leigh Syndrome associated with complex I deficiency.

2 Results

Development of *C. elegans* models for human mitochondrial associated diseases

To develop new models for HMAD we silenced a panel of 42 *C. elegans* genes orthologous to nuclear-encoded genes that when mutated in humans lead to severe mitochondrial dysfunction and neuro-developmental pathologies [17, 22]. Two independent rounds of screen were carried out for two consecutive generations in search of those dsRNA clones giving the characteristic phenotypic effects associated with different degrees of mitochondrial stress (**Figure 1a; Table I**): i) a “mild” gene suppression causing slight decrease in size and fertility and slow development - phenotypes previously associated with a beneficial pro-longevity mitochondrial stress response [21, 24]; and (ii) a “strong” gene suppression inducing animals’ sterility, growth arrest or lethality, reflecting the deleterious effect ascribed to severe mitochondrial dysfunction. Most of the clones screened showed a "mild" phenotype in the parental generation and a "strong"

phenotype in the second generation (**Figures 1b**). When a "strong" phenotype was already observed in the parental generation, animals were fed with a diluted dsRNA-expressing bacterial clone to obtain a "mild" phenotype (**Figure 1c**). 20 clones gave consistent and very reproducible results on development and fertility upon different degrees of mitochondrial stress and were selected for further characterization. Surprisingly, when lifespan was analyzed, most of the genes with a few exceptions (e.g. *pdr-1*), actually elicited a greater lifespan extension when more severely suppressed, although with clear trade-off effects on fertility or development as expected by a disease state (**Figure S1; Table SI and SII**). This indicates that, consistent with our recent observation [24], health-related features such as fertility and development reflect the severity of animals' mitochondrial disruption better than lifespan. Given their very strong and reproducible phenotype (L2/L3 larval arrest), and health importance in humans (frequency of mutation), we then decided to focus on animals with severe suppression of complex I (genes labeled in red in **Table I**) and further characterized features relevant for the human disorder.

Severe suppression of Complex I genes impairs neuronal and mitochondrial functionality

Most complex I defects are associated with Leigh Syndrome, a devastating neuromuscular degenerative disorder with early childhood onset and no cure [6]. Using different chemicals, which in *C. elegans* are sensed by different sub-classes of neurons [25, 26], we assessed animals sensory function in larvae and found that strong suppression of the different complex I subunits caused, similar to a disease state, a very severe neuronal impairment compared to stage-matched controls (**Figure 2a,b; Figure S2a-d; Table SIII**). The neurosensory defect was very specific as sensitivity to a "gentle touch" mechanical stimulus [27, 28] was not altered, at least when checked in *nuo-5* and *lpd-5* mutants (*data not shown*). Besides the neurodevelopmental defects Leigh Syndrome disease typically manifests with rapid deterioration of the motor function. To our surprise, when we monitored animals' ability to move by counting the number of body bends

per minute in solid agar plate [26, 29], severe suppression of mitochondrial proteins did not significantly reduce animal speed compared to wild-type animals (**Figure S2e**), with the exception of one clone, *nuo-1*. Yet, notably, similar to the perceived fatigue often observed in patients with mitochondrial disorders [30], a locomotion defect could be revealed under energetic challenge, a condition that in *C. elegans* can be simulated by swimming [31] (**Figure S2f**).

To characterize different aspects of mitochondrial metabolism, we then further narrowed our study to two complex I subunits, namely LPD-5, a 18-kDa subunit also involved in fat storage and NUO-5, a 75-kDa subunit thought to be the first of many Fe-S proteins to accept electrons from an NADH-flavoprotein reductase. Mitochondrial respiration was measured with the Seahorse Bioscience Flux Analyzer [32] and optimized for nematodes at L2/L3 larval stage [24]. Consistent with a mitochondrial disease state, all parameters associated with mitochondrial respiration were affected upon severe suppression of *nuo-5* and *lpd-5* compared to wild-type animals. Specifically, basal oxygen consumption rate (OCR), maximal respiratory capacity (upon treatment with the uncoupling agent carbonyl cyanide 4-trifluoromethoxy-phenylhydrazone), ATP-linked OCR (in the presence of the ATP inhibitor Dicyclohexylcarbodiimide) as well as steady-state ATP levels, were all significantly reduced (**Figure 2c-f)**. Spare respiratory capacity (resulting by subtracting basal from maximal OCR), which indicates organism's ability to respond to increased energy demand, and proton leak, were however only significantly reduced in *nuo-5*-depleted animals (**Figure S3a,b)**. We also found that *nuo-5* and *lpd-5* RNAi-treated animals produced significantly more reactive oxygen species (ROS) (**Figure 2g**). However, to our surprise, we could not reveal any major oxidative damage: *nuo-5* and *lpd-5* RNAi did not increase the expression of a classical sensor of oxidative stress (p38MAPK/*pmk-1*, **Figure S3c**), and actually reduced both lipid and amide oxidation (**Figure**

2h; Figure S3d). Moreover, although mitochondrial DNA is especially sensitive to oxidative damage [33], *nuo-5* and *lpd-5* RNAi-depleted animals only present with nuclear but not mitochondrial DNA damage (**Figure S3e,f**); and quantitative measurements of mitochondrial genome copy number, which can also be oxidative stress-responsive [34], also did not reveal any significant difference between control and RNAi-treated animals (**Figure S3g**). These results suggest that these animals up-regulate stress response defensive mechanisms. Indeed, we observed that *nuo-5* and *lpd-5* RNAi increased the expression of genes involved in mitochondrial quality control pathways [22, 35, 36]: the antioxidant response gene glutathione S-transferase *gst-4*, the mitochondrial unfolded protein response gene *hsp-6*, and the mitophagy regulator Bnip3 homolog *dct-1* (**Figure 2i-k; Figure S4a**). Disturbing *C. elegans* mitochondrial function also induces autophagy, lipid remodeling [37] as well as drug detoxification and pathogen-response genes [38]. Accordingly we observed that the nuclear translocation of HLH-30, a common regulator of these 'cytoprotective' pathways [39, 40], was also significantly increased in *nuo-5* and *lpd-5* arrested L3 animals (**Figure 2l**) - differently from *daf-2* RNAi that only promoted HLH-30 activation in adults but not in the L3 larvae (**Figure S4b**). Taken together, characterization of our new models for complex I deficiency indicates that, similar to the human disease, animals with strong *nuo-5* or *lpd-5* suppression present with severe developmental, neuromuscular and mitochondrial defects, surprisingly without displaying overt oxidative damage.

To start gaining insight into the molecular mechanisms accounting for the deleterious effects associated with severe mitochondrial dysfunction, we compared the transcriptomic profile in control L3 larvae with that of mild or strong (arrested) *nuo-5* RNAi (**Figure 3a**). Remarkably, as opposed to what has been observed in the adults [41-44], mild mitochondrial stress lead to very few changes in gene expression in the L3 (only four genes, *fmo-2, B0205.13, T16G1.6 and nuo-*

5, were differentially expressed based on a relatively liberal FDR-corrected $p < 0.05$ cut-off). Moreover, consistent with the different degree of mitochondrial dysfunction upon different degrees of mitochondrial stress, the 303 genes differentially expressed uniquely between mild and severe *nuo-5* treatments all belong to GO terms associated with mitochondria (**Figure 3b,d; Figure S4c**), clearly indicating that the metabolic alterations we previously observed in response to mild mitochondrial stress [24] precede genomic reprogramming. Thus at least at this stage, the mitochondrial remodeling appears to successfully compensate for the genetic deficiency, obviating the need for detectable transcriptional changes to other parts of the cell. In contrast, large transcriptomic changes are triggered in larvae upon severe mitochondrial stress. Interestingly, the 1152 genes uniquely different between control and strong *nuo-5* suppression, reveal GO terms (**Figure 3c,e; Figure S4d**) affecting multiple cellular compartments, from nucleus to cytoplasm to the Golgi apparatus and membrane components, as well as genes involved in lifespan determination, ribonucleoprotein complex biogenesis and neuropeptide signaling, thus showing a more general cellular remodeling not only limited to mitochondria.

A phenotype-based screening identifies Lutein as a Complex I disease suppressor

In vivo genetic and compounds screening with model organisms exponentially grew in the past decade as strategies to identify modifiers of specific phenotypes ranging from proteins expression to mitochondrial function and animals' behaviors [11, 45, 46]. Natural compounds supplemented through the diet may especially provide more feasible therapeutic opportunities than genetic or pharmacological interventions. We took advantage of the reproducible, discrete and quantifiable disease-relevant phenotype – developmental arrest – observed in our complex I disease models to screen a small library of mainly (but not only) natural compounds in search of potential disease suppressors. We first used two different approaches to verify the possibility of rescuing the developmental arrest induced by severe knock down of complex I proteins, as this

might be irreversible or require a treatment at a specific stage in order to be prevented or rescued. In the first approach we took advantage of the *C. elegans* p53 ortholog mutant, *cep-1(lg12501)*, which can prevent the developmental arrest induced by severe suppression of *nuo-2* and of other mitochondrial proteins [23]. Lack of *cep-1* also partially rescued the development arrest observed in different disease models (**Table SIV**), indicating the arrest is indeed a reversible phenotype. In the second approach, we moved the F1 progeny from disease-inducing RNAi back to control (empty vector-expressing) bacteria at different stages, from eggs to L3. Depending on the disease model, the developmental arrest could be prevented moving the animals on control bacteria from eggs to L2, but in most cases not after L3 arrest (**Figure S5a; Table SIV**), with obvious implications for the efficacy of a possible therapeutic approach.

A total of 37 compounds were then supplemented at different concentrations (ranging from 0.5 µM to 1 mM) to the second generation of animals (starting from eggs) fed UVB-killed bacteria transformed either with control vector or with *nuo-5* or *lpd-5* dsRNA (**Figure S5b**). Among tested conditions, 11 were able to partially prevent the arrested phenotype of *nuo-5*-depleted animals while 7 rescued that of *lpd-5*-depleted animals, resulting in a total of 11 compounds which allowed more than 20% of worms to develop into adults after 6 days of treatment (**Figure 4a,b; Figure S6a,b; Table SV**). We excluded the possibility that the most relevant compounds affected the efficacy of the RNAi rather than preventing their deleterious effects, by verifying that they were not able to suppress the embryonic lethality induced by unrelated *skn-1* or *phi-7* RNAi (**Figure S7a-b**). Moreover, lutein absorbance peak at 1515.8 cm^{-1} [47] in the worms, detected through infrared microspectroscopy, confirmed that they uptake the drug (**Figure S7c**). Finally, we looked at the effect of lutein, macrosporin and isovitexin on development from day 4 to 6 and observed that the effect of lutein was the most reproducible and significant (**Figures**

S8a-d; **Figure 4c**). We thus decided to follow up on lutein, which we also specifically excluded to interfere with *nuo-5* RNAi potency (**Figure S7d**).

Lutein suppresses behavioral and cellular defects in models of Complex I deficiency

Lutein is a carotenoid belonging to the xanthophyll family that is found abundantly in leafy dark green vegetables, egg yolk, animal fat and human eye retinal macula [48]. Increasing evidence points towards the beneficial effects of lutein in several pathological conditions, ranging from cancer to neurodegenerative disorders [49-52]. Strikingly, we found that lutein not only partially rescued the developmental defect of complex I disease animals (**Figure 4c**), but also substantially ameliorated their neuronal deficits (**Figure 4d-g**). Specifically, treatment with lutein significantly improved the chemotaxis defect of *nuo-5*- and *lpd-5*-depleted animals towards different chemicals, in some cases even above the level of wild-type lutein-treated animals. Indeed, lutein enhances the sensory neuron functions in the control worms, but this improvement was greatly accentuated in the *nuo-5* and *lpd-5* mutants (**Figure 4d-g**).

The most likely physiological functions of this pigment in macular membranes are protection against oxidative and radiation induced damage of the lipids [53, 54]. Accordingly, lutein was able to decrease ROS amount in *nuo-5*- and *lpd-5*-depleted *C. elegans* and in cell lines derived from patients carrying mutations in their human homologs NDUFS1/*nuo-5* and NDUFS4/*lpd-5* [4] (**Figure 4h-I; Figure S9a,b**). Lutein also significantly reduced *dct-1* expression (at least in *nuo-5* depleted animals) (**Figure S9c,d**) and completely prevented *hlh-30* activation (**Figure 4j**), which might have been increased either by ROS or mitochondrial damage. However, it did not affect oxidation of cellular components and failed to protect against oxidative stress in *C. elegans* (**Figure S9e-g**), which, along with above described results suggest ROS-induced damage may not play a major role in disease-associated defects. In line with this possibility, lutein did not suppress the induction of mitochondrial stress response genes *gst-4* and *hsp-6* (**S9h,i**). Taken

together, our findings revealed that lutein ameliorates developmental, neuronal and cellular dysfunction in NDUFS1/*nuo-5*-associated disease model, most likely through indirect effects on downstream mitochondrial modulated processes rather than through direct beneficial effects on mitochondria or as an antioxidant.

Lutein rescues a newly identified synaptic defect in NDUFS1/*nuo-5*-depleted animals

To gain insight into possible protective molecular mechanisms of lutein, we compared the transcriptomic profile of stage-matched (L3) cohorts of *C. elegans* upon strong *nuo-5* RNAi, treated and untreated with lutein, with that of animals fed empty vector control. The comparison between wild-type and *nuo-5* RNAi-depleted animals revealed 2274 altered genes, implicated in fundamental cellular morphogenesis processes and especially, as expected, in organismal and nervous system development (**Figure S10a; Table SVI**), reflecting the very strong effect of the treatment on worm's biology ultimately leading to arrested growth. On the other hand, interestingly, when comparing wild-type animals with *nuo-5* treated with lutein (rescued animals), the number of altered genes diminished to 1296, indicating that roughly half of the genes are restored to wild-type levels. Notably, most of these genes belong to developmental and neuronal processes, consistent with the partial rescue of the arrested development and neuronal function observed upon lutein treatment (**Figure S10b; Table SVI).** We then focused our attention on the differences between *nuo-5*-depleted worms and *nuo-5*-depleted animals treated with lutein, and identified 143 differentially expressed genes (**Figure 5a,b; Table SVI**). Intriguingly, the gene ontology analysis revealed four main pathways enriched upon lutein treatment: (i) secretion (synaptic and neurotransmission regulation), (ii) endosomal transport, (iii) protein import into the nucleus and (iv) mitotic sister chromatin segregation (cell cycle), (**Figure 5c**). Analysis of *nuo-5* expression in the microarray data supports previous qPCR results

(**Figure S7**) and establishes that lutein-rescuing effects are specific and not ascribed to a reduced potency of the *nuo-5* RNAi (**Figure S11a**).

In light of the microarray data and of the severe neuromuscular defects observed in human patients with Leigh Syndrome and in our *C. elegans* model, we speculated that defective mitochondria affected synaptic vesicle trafficking and consequently synaptic functionality, which is somehow rescued by lutein. To address our hypothesis, we took advantage of behavioral assays commonly used to assess synaptic functionality in *C. elegans* [55-59]. Mutations affecting synaptic transmission lead to altered resistance to aldicarb, an acetyl-cholinesterase inhibitor [56]: mutants with increased cholinergic synaptic transmission are hypersensitive to aldicarb and paralyze faster than wild-type animals (Hic phenotype), while mutants with reduced cholinergic synaptic transmission have increased resistance to aldicarb and take longer time to become paralyzed (Ric phenotype) upon aldicarb treatment. Strikingly, in support of our hypothesis, we identified for the first time a synaptic defect in *nuo-5*-depleted animals, which indeed paralyzed faster than wild-type in the presence of the same concentration of aldicarb, indicating an increased cholinergic transmission. Most notably, when *nuo-5* worms were treated with lutein from eggs throughout L3 larvae they lose the Hic phenotype and have an attenuated response to Aldicarb (**Figure 6a; Figure S11b**).

The Hic phenotypes could be ascribed either to pre-synaptic alterations, such as inability to negatively regulate pre-synaptic ACh release or reuptake, or to post-synaptic defects, like loss of post-synaptic ACh regulation or inhibitory GABA transmission. Since the aldicarb assay does not distinguish between these different scenarios we took advantage of levamisole, a selective agonist of the nicotinic acetylcholine receptors found at the postsynaptic side of the neuromuscular junction (NMJ) [57]. Wild-type nematodes exposed to levamisole paralyze over time due to excessive excitation of the acetylcholine receptors and worms with mutations in

these receptors are usually more resistant to levamisole. Instead, animals with mutations affecting presynaptic function paralyze either in a similar rate or slightly faster than wild-type on levamisole plates (due to a possible postsynaptic increase in cholinergic receptors expression or function) [60, 61]. Interestingly, we found that *nuo-5* deficient worms are also paralyzed faster than wild-type animals in response to levamisole, and this paralysis was in part reverted by lutein (**Figure 6b**). These data are consistent with an exaggerated presynaptic activity in *nuo-5*-depleted animals and point towards lutein protective effect at the presynaptic level or in the synaptic cleft. The partial effect of lutein on levamisole-induced paralysis, is possibly due to an over excessive levamisole concentration and/or to activation of postsynaptic receptor compensatory mechanisms or to a concomitant defect in the GABA inhibitory system.

To discriminate between these different possibilities, we took advantage of a complementary assay, which exploits pentylenetetrazole (PTZ) [58], a GABA receptor antagonist. In response to PTZ, neurotransmission mutants display different phenotypes: wild-type worms and mutants with defects in ACh release do not display PTZ sensitivity, due to appropriate regulation of ACh amount and activity; mutants that cannot negatively regulate ACh release, and thus secrete excessive amounts of ACh become completely paralyzed upon PTZ treatment [58]; GABA receptors mutants (e.g. *unc-49*), instead only display dose-dependent paralysis of the body (but not of the head) resulting in head convulsions (head bobs). We found that *nuo-5*-depleted worms responded to PTZ with a significantly higher percentage of full-body paralysis, and only a small non-significant fraction of head convulsions (**Figure 6c; Figure S11c,d**). This response is typically associated with the inability to negatively regulate ACh release, and excludes a major defect in GABAergic transmission [59]. Most importantly, lutein treatment significantly suppressed the full body paralysis but not the head convulsions (**Figure 6c; Figure S11c,d**), clearly indicating a rescuing effect of the altered negative feedback on ACh release (**Figure 7**).

Neuroligin mediates the protective effect of Lutein on cholinergic synapses

We then turned to our microarray results to identify possible lutein downstream molecular players. We confirmed the effect of lutein on different *nuo-5* RNAi-induced genes, such as *vps-35*, *nlp-40* and *unc-10* (**Figure S11e**), highly representative of the two main GO categories (**Figure 5c**) and exploited GFP reporter strains to analyze the expression of different genes involved in synaptic functionality. The expression of UNC-10 a protein involved in synaptic membrane exocytosis, was significantly induced in *nuo-5*-depleted animals and suppressed by lutein (**Figure 6d, Figure S12a**). The expression of *glb-10*, which is required for synaptic structure and functioning [62, 63], was reduced in the mutant worms and returned to levels similar to control upon lutein treatment (**Figure 6e; Figure S12b**). *unc-17*, a gene required in cholinergic neurons to load acetylcholine into synaptic vesicles, was increased in *nuo-5*-depleted animals (**Figure 6f; Figure S12c**) and reduced to control levels upon lutein treatment. Finally, the expression of *nlg-1*, coding for the presynaptic cell adhesion protein neuroligin (NLG-1), which along with postsynaptic neurexin (NRX-1) mediates in *C. elegans* a retrograde signal that inhibits neurotransmitter release at NMJ [64], was significantly increased in *nuo-5*-depleted animals and goes back to wild-type levels upon lutein treatment (**Figure 6g; Figure S12d**). These observations along with the behavioral assays, are indicative of an excessive buildup of ACh in the synaptic cleft in the disease model, a defect that is drastically rescued by lutein.

Up-regulation of *nlg-1* is required to enhance synapses strength and prevent neuronal degeneration in response to oxidative stress [65]. We thus reasoned that *nlg-1* is upregulated by *nuo-5* depletion to compensate for a mitochondrial-stress-induced synaptic defect, and its downregulation upon lutein treatment likely represents a consequence of lutein beneficial effects on neuronal transmission. In this scenario knock-out of *nlg-1* should worsen the deleterious effects of *nuo-5* RNAi, but lutein may still retain some beneficial effects. Strikingly, contrary to

our expectation, *nlg-1* knockout ameliorated neuromuscular (trashing, sensitivity to aldicarb and levamisole, as well as full body paralysis in response to PTZ**, Figure 6h-k; Figure S12e-h**) as well as developmental defects (**Figure 6l**) observed in the disease model. These results imply that induction of *nlg-1*, contrary to the protective effect that has been observed against oxidative stress [65], has instead a detrimental effect when upregulated in response to mitochondrial dysfunction. Moreover, they suggest that lutein may exert its beneficial effect by reducing *nlg-1* expression. According to this scenario, *nlg-1* knock-out clearly masked the beneficial effects of lutein (**Figure 6h-l; Figure S12e-h**).

3 Discussion

In the present work, we developed and systematically characterized new *C. elegans* models for HMADs, and focused on mitochondrial complex I-deficiency to carry out a phenotype-based screening in search of disease suppressors. We identified a natural compound, lutein, which significantly rescued most of the neurodevelopmental deficits we observed in two models of complex I deficiency associated with Leigh Syndrome, NDUFS1/*nuo-5* and NDUFS4/*lpd-5*. Importantly, we found that lutein exerts its effect through suppression of a synaptic defect, which we described for the first time in NDUFS1/*nuo-5*-depleted animals. We specifically identified the *C. elegans* neuroligin homolog, *nlg-1*, as a novel culprit of the neuronal cholinergic defect observed in this disease model and as a potential target for lutein's protective effect (**Figure 7**). With a few exceptions, experimental models for complex I disorders and especially for Leigh Syndrome associated with NDUFS1 mutations do not exist or do not fully recapitulate the disease state [66-69], thus seriously hampering the development of adequate therapeutic strategies, which indeed are not available for these devastating, life threating disorders. As a consequence, studies revolved at investigating complex I disorders and

potential therapeutic strategies are primarily carried out in patients' fibroblasts or lymphoblasts, which, although certainly useful, are not the most relevant systems to recapitulate diseases of the nervous system. Therefore, in the first part of this work, to generate new HMAD models, we carried out a customized RNAi screen of genes whose severe deficiency in human is associated with mitochondrial disorders. We identified for half of the clones under study a dose-dependent response to the gene silencing, which nicely mimic the disease progression and is consistent with the mitochondrial threshold effect. Namely, compensatory pathways may help coping with a mild mitochondrial stress, yet, after a certain threshold of mitochondrial dysfunction is reached, these pathways are no longer protective and detrimental features arise, such as mitochondrial and neurodevelopmental deficits [8, 21, 22, 24, 29]. Surprisingly, we found that animals with mild and severe mitochondrial disruption were in most cases equally long-lived compare to wild-type, indicating that signaling pathways specifying development and lifespan upon mitochondrial stress are uncoupled. Indeed, our gene expression profiles in the L3 larvae indicated that remodeling of mitochondrial structure and function underlie the main (developmental) differences observed between mild and strong *nuo-5* suppression. Yet, changes in lifespan-regulatory pathways normally observed in adult upon mild mitochondrial stress [41-43], are not observed in the L3, while are already visible upon severe mitochondrial suppression. Along with the respiration profiles, these data support previous works indicating that mitochondrial changes are not all relevant for longevity specification [24, 44, 70, 71]. Severe suppression of different HMAD genes induced very consistent *C. elegans* phenotypes (developmental arrest or reduced body size), which were essential to carry out our suppressor screen but consistent with the heterogeneity of signs and symptoms of these mitochondrial disorders, we also observed variable phenotypic changes. Suppression of different genes indeed lead to differences in the extent of locomotion and of chemosensory deficits, in mitochondrial respiration parameters, in the ability

to rescue the developmental arrest elicited by compounds or by p53/*cep-1* depletion. Moreover, upon suppression of complex I subunits, we also observed very specific phenotypes, such as alteration of chemosensory but not touch sensory function or basal locomotion activity. We initially assumed the movement defects simply arise at a later age, as previously observed [29], but we could actually uncover it under increased energetic request [31]. Interestingly, this behavior is very similar to the perceived fatigue often observed in patients with mitochondrial disorders [30] and given the suppressive effect of lutein, it provides us with a very sensitive and quick assay for future suppressor screening. It will be important to further investigate whether complex I deficiency or suppression of other HMAD genes increases sensitivity to metabolic or environmental stressors as these factors may influence mitochondrial activity and have devastating consequence on patients with Leigh Syndrome or other mitochondrial-associated disorders [72, 73]. Of note, although we observed increased ROS production in both *C. elegans* and patients' fibroblasts, accompanied by increased expression of stress response genes (e.i. *gst-4*, *hlh-30*, *dct-1*, and *hsp-6*) and increased sensitive to oxidative stress in *nuo-5*- and *lpd-5*-depleted animals, oxidative damage does not seem to play a major role in disease model outcomes and suppression. In fact, proton leak as well as lipid and amide oxidation were actually reduced and a classical oxidative stress response gene (p38MAPK/*pmk-1*) was not activated in the disease models. Furthermore, while lutein significantly suppressed neurodevelopmental deficits, as well as the induction of *hlh-30* and *dct-1* in the two disease models, it neither suppressed the induction of *gst-4* or *hsp-6* nor modulated oxidative stress response. Thus, *hlh-30*/TFEB-regulated autophagy and *dct-1*/Bnip3-regulated mitophagy may represent protective mechanisms against the mitochondrial defects or induce deleterious effects if over-activated by the disease state. Regardless, their repression may be seen as part of a cytoprotective effect promoted by lutein. Autophagy and mitophagy have been already implicated in the pathogenesis

of different neuromuscular disorders and it will be important to establish their exact role in HMAD pathogenesis.

Remarkably, through a combination of genetic and behavioral assays we were able to narrow down the neuronal defect in our Leigh Syndrome model and to uncover for the first time an acetylcholine presynaptic alteration (most likely an impairment in the ability to negatively regulate ACh release at the NMJ), which was significantly suppressed by lutein treatment. Of note, both mitochondria and autophagy play critical role in shaping synaptic structure and function [74-78] and our microarray data pointed towards genes regulating neurotransmitter secretion and endosomal transport as two out of four main pathways affected by lutein in the disease model. It will be thus very interesting to investigate how the mitochondrial dysfunction in this disorder is actually causing the synaptic alteration and whether autophagy, which we found to be causally involved in mitochondrial stress control of longevity [37, 79], plays a role in this context. Intriguingly, we showed that within different synaptic regulatory genes affected by *nuo-5* depletion, lutein treatment consistently and significantly suppressed the upregulation of neuroligin (*nlg-1*), a cell adhesion synaptic protein that along with its partner protein neurexin, mediate a retrograde synaptic signaling that inhibits neurotransmitter release [64, 80, 81]. Unfortunately, despite different attempts, we were unable to validate in patients fibroblasts the gene expression changes observed in the *C. elegans* disease model (*data not shown*), as these most likely primarily reflect neuronal alterations. While we still don't know how *nlg-1* is upregulated in our model, it is worth noting that *skn-1* (homolog of the Nrf2 redox transcription factor)-mediated *nlg-1*-induction, in neurons, confers resistance to oxidative stress [65]. According to this scenario, in our disease model *nlg-1* would be induced to protect against severe mitochondrial dysfunction and its depletion would worsen the detrimental effects of *nuo-5* RNAi. Yet, very interestingly, *nlg-1* knock-out partially rescued the developmental and neuronal

deficits in the disease model and also masked the beneficial effects of lutein. Moreover *nuo-5* and *lpd-5* depleted animals were actually more sensitive to oxidative stress and lutein, which has been shown to activate Nrf2/*skn-1* in mammals [82], neither affected this response, nor suppressed *nuo-5* RNAi-mediated induction of *gst-4* (a well-established *skn-1* target in response to oxidative stress). Thus, although we cannot rule out context specific effects of *skn-1*-mediated induction of *nlg-1*, our findings indicate *nlg-1* overexpression in this disease context has a actually a detrimental rather than a protective effect. This effect is suppressed by lutein, most likely through ROS-independent mechanisms modulated downstream to mitochondria.

Mitochondria regulate synaptic activity in many ways and severe mitochondrial dysfunction is therefore expected to have broader repercussion on synaptic regulatory proteins [74]. Increased expression of NLG-1 may thus represent a neuronal attempt to compensate for compromised synaptic signaling induced by the mitochondrial disruption. However, rather than protective, this would lead to a pathological synaptic excitation, which, as supported by our transcriptomic and behavioral (aldicarb, levamisole and PTZ sensitivity) data, was in fact rescued by lutein suppression of NLG-1 overexpression (**Figure 7**). Chronic exposure to lutein in the diseased worms could thus activate NLG-1-regulated compensatory mechanisms that rescue their paralysis defects. Interestingly, NLG-1 contains an extracellular cholinesterase-like domain that forms the interaction with the neurexin domain [83], and lutein was shown to have acetylcholinesterase (AChE) inhibitory activity [84-86]. Whether lutein neuroprotection in this disease model is mediated by direct inhibition of synaptic AChE and/or NLG-1 activity (in turn suppressing compensatory *nlg-1* overexpression), is an attractive possibility that require further investigation. It is worth noting that Alzheimer's disease (AD) patients were reported to have significantly less macular pigments (comprising lutein, zeaxanthin and meso-zeaxanthin) and lower serum concentrations of lutein and zeaxanthin compared to control subjects [87] and that

AChE inhibitors are the standard therapy for AD [88]. Moreover lutein was shown to have beneficial effects against AD [51] as well as against other neuropathological conditions such as diabetic retinopathy [52], age-related macular degeneration [50], ischemia [89] and Parkinson disease [90], primarily due to its antioxidant, anti-apoptotic and mitochondrial protective properties. We provide for the first time the proof of principle for considering lutein as a new and easily accessible therapeutic for mitochondrial diseases associated with complex I deficiency, which to date present with no cure. Lutein can be naturally ingested through the diet (dark leave vegetables), as a dietary supplement or as an ingredient in nutraceutical foods. However, due to its highly hydrophobic nature different strategies are being developed to improve its bioavailability [91-93], which can therefore offer more effective therapeutic strategies. Finally, besides lutein, our suppressor screen identified few other compounds that partially rescued the developmental arrest of complex I deficient animals and it will be important to assess them alone or in combination with lutein in the different neuronal assays.

In summary, in this work we established new powerful animal models for complex I deficiency-associated diseases, devastating neurodevelopmental disorders which do date present with no cure, with a particular focus on NDUFS1-associated Leigh Syndrome (to our knowledge the first and only animal model for this disease). We used the new models to support the growing body of evidence indicating that live animal screens are ideal tools for drug discovery strategies designed to identify suppressors of specific disease-associated phenotypes [46, 94, 95]. Most importantly, although validation in mammalian systems or humanized animal models will be required to fully support our findings, we provided for the first time the rationale for suggesting lutein as a novel therapeutic to rescue a cholinergic synaptic dysfunction we identified for the first time in this Leigh syndrome disease model associated with mitochondrial complex I deficiency.

4 Methods

C. elegans methods

C. elegans strains and maintenance

We employed standard nematode culture conditions [96]. All strains were maintained at 20 °C on Nematode Growth Media agar supplemented with Escherichia coli (OP50 or transformed HT115), unless otherwise indicated. *S*trains used in this work are: N2: wild-type (Bristol), $p_{glb\text{-}10}$::GFP; SJ4100:zcIs13[$p_{hsp\text{-}6}$::GFP], CL2166 dvIs19 [(pAF15)$p_{gst\text{-}4}$::GFP::NLS] III, JIN1679: jinEx10 [$p_{hlh\text{-}30}$::HLH-30::GFP + *rol-6*(su1006)], LX929:vsIs48 [$p_{unc\text{-}17}$::GFP], PE255:feIs5 [$p_{sur\text{-}5}$::luciferase::GFP + *rol-6*(su1006)] X, IR1431: N2;Ex001[$p_{dct\text{-}1}$DCT-1::GFP], AU78: agIs219 [T24B8.5p::GFP::unc-54-3' UTR + ttx-3p::GFP::unc-54-3' UTR] III [2], KP3928 nuIs165 [punc-129::UNC-10::GFP], VC228: nlg-1(ok259) X, vjIs47[pnlg-1::GFP]IV [3] and CB407: unc-49(e407) III [4].

RNAi feeding

The following dsRNA transformed bacteria for feeding were derived from the Ahringer *C. elegans* RNAi library [97]: *nuo-1* (C09H10.3), T20H4.5, F53F4.10, *cco-1* (F26E4.9), *nuo-5* (Y45G12B.1), *nuo-2* (T10E9.7), *spg-7* (Y47G6A.10), *lpd-5* (ZK973.10). For additional RNAi used in the phenotypic screening described in the text refer to Table I. All dsRNA bacterial clones (which were sequence validated), were grown to a concentration of 0.9 OD and diluted 1/10 or 1/50 (where indicated) with empty vector expressing bacteria as previously described [21].

Chemotaxis assays

Animal's neurons functionality was assessed by quantifying attraction or repulsion to different concentration of chemicals as follow: sodium azide (NaN_3), used to anesthetize worms, was placed on buffered agar 180 degrees opposite on a 10 cm dish; the attractant (or repellent) was then placed on one NaN3 spot, and ethanol (neutral odor for the worms in which chemical was diluted) on the other spot; a population of 80-100 age-synchronized animals was placed in the center of the testing plate and the number of worms at attractant and control was counted every 15 minutes for four hours to calculate the Chemotaxis Index (CI). CI=(A-B)/(A+B+C), where A is the number of worms at attractant, B is the number of worms at control and C is the

number of animals which didn't reach any of the two spots at the end of the two hours. For a population of 3 days old, wild-type animals, a good CI is around 0.8 for attractants and –0.8 for repellents after two hours (CI=0 means no attraction, while CI=1 or –1 represent maximum attraction or repulsion, but there are always some animals that, also for a wild-type strain, remain randomly dispersed in the assay plate or reach the control spot instead of the attractant) [26]. Compounds used in chemotaxis assays were all acquired from Sigma-Aldrich: ammonium acetate (**A1542)**, was diluted in distillated water and 2-Methyl-3-(methylthio)pyrazine (**545791)**, 1-Butanol (9**B7906)**, Benzaldehyde (**418099)**, all diluted in Ethanol 99.8%.

Body bend

Locomotion was assessed by counting the number of body bends (changes in the body bend at the mid-body point per minute), per minute for each worm on solid agar plates with no bacteria. One bend was counted every time the mid-body reached a maximum bend in the opposite direction from the bend last counted. Body bends were checked in at least 20 single worms in 2 or 3 independent biological trials [26].

Thrashing assay

To further define neuro-muscular differences and on an individual level, we analyzed the swimming behavior (also known as thrashing) **[98]** of *nuo-5* animals . Age-synchronized worms were transferred to a fresh unseeded plate at room temperature to remove leftover bacteria; then individual worms were transferred to an unseeded small NGM plate filled with 1 mL of S-Basal buffer. Worms were allowed to acclimatize for 5 minutes, and the number of completed thrashes per minute was counted using a hand counter. This was performed on 15 individual worms per replicate in 2 or 3 independent biological trials.

Lifespan assay

Lifespan and Statistical Survival analysis using synchronous populations of at least 60 animals per strain. Survival curves and statistical analyses were carried out as previously described [23]. Survival analysis started from hatching and was carried out at 20°C. Animals were scored as dead or alive and transferred every day on fresh plates during the fertile period, and then every other day or every 3 days until death. Worms were considered dead when they stop pharyngeal pumping and responding to touch. Worms that died because of internal bagging, desiccation due to crawling on the edge of the plates, or gonad extrusion were scored as

censored. These animals were included in lifespan analyses up to the point of censorship and were weighted by half in the statistical analysis. We calculated mean lifespan, standard deviation of the mean, and P value (Mantel-Cox regression analysis) from Kaplan-Meyer survival curves of pooled population of animals coming from at least two independent replicas. For statistical analysis we used the Online Application for Survival analysis OASIS 2 [99]. See Table S1 for the summary of lifespan.

Measurement of respiration using the Seahorse XF Analyzers

The fundamental parameters of mitochondrial respiratory chain, including basal oxygen consumption rate (OCR), maximal respiratory capacity, spare respiratory capacity, ATP coupled respiration and proton leak, have been assessed with pharmacological inhibitors of the electron transport chain (ETC) using the Seahorse XFe24 Analyser (Seahorse Bioscience, Massachusetts, USA). Briefly, all measurements were performed with synchronized L2-L3 *C. elegans.* As the "strong" treatment with RNAi against the mitochondrial proteins under study (namely, *nuo-5* and *lpd-5*) lead to arrest animal development at L2/L3 larval stage we decided to carry out all the Seahorse measurement at this developmental age. Synchronized wild-type (*N2)* worms were grown at 20°C for two consecutive generations on bacteria expressing dsRNA against the genes of interest: *nuo-5* and *lpd-5*. Mitochondrial respiration from these animals was compared with stage-matched animals left untreated or fed for only one generation (mild treatment). The Seahorse Bioscience Flux Analyzer was programmed with the appropriate protocol [100]. Worms were rinsed off the plate and washed and the number of animals estimated (by counting the number of worms in 20µl drops under a dissecting microscope). The 24-well Seahorse Cartridge was loaded with nearly 250 nematodes pipetted into each well. The final volume of each well was brought to 525µl with unbuffered EPA water. Two wells per assay were filled with EPA water without worms and used as blanks. 75 µl of each drugs were loaded into the designated injection ports of the seahorse cartridge. The final solution concentrations after injection of each drug being the following: 20µM DCCD (1% DMSO), 25µM FCCP (2% DMSO), and 10mM azide. The OCR was normalized to the actual number of worms in each well and the values obtained were again normalized on the actual protein content per worms measured with a BCA protein assay after sonication of 2000 nematodes for each condition. The average and the standard error of OCR per worm across the five replicates for each sample were calculated and a minimum of 10 time points of 5 wells was used.

Measurement of ATP levels

The intracellular ATP levels were assessed quantifying the whole animal luminescence in the *C. elegans* strain PE255 [101-103]. This Strain is bioluminescent when provided with exogenous D-luciferin (potassium salt) due to the presence of the *sur-5* promoter driving expression of firefly (Photinus pyralis) luciferase (lacking the peroxisome tagging signal) fused in-frame to GFP (S65C). The measurements were carried out as in [104]. Briefly, worms at the desired developmental stage (L2/L3 larvae) were transferred to 15mL conical tube, spun at 2200 RCF and the supernatant was removed. Nematodes were resuspended in k-medium to a concentration of 1.0±0.2 nematodes/µl. 50-100 animals were pipetted into each well of a white 96-well plate (4-5 wells per treatment), and brought to a final volume 100uL with k-medium. K-medium alone was used for blank measurements. A plate reader was used to read first the GFP fluorescence (Emissions filter: 502nm; excitation filter: 485nm) and then the luminescence after injection of a luminescence buffer. The ATP production was then calculated dividing the luminescence signal by the GFP intensity.

Analysis of mitochondrial DNA copy number, mitochondrial DNA and nuclear DNA damage

Synchronized wild-type (*N2)* worms were grown at 20°C for two consecutive generations on bacteria expressing dsRNA against the genes of interest: *nuo-5 and, lpd-5*. nDNA and mtDNA from these animals was compared with stage-matched animals fed bacteria expressing the empty vector pL4440.

Six worms were picked and pooled in a single tube per biological replicate, and three biological replicates were taken per treatment in three experiments separated in time.

nDNA and mtDNA damage have been evaluated using a quantitative PCR (QPCR)-based method as previously described in [105, 106]. This assay defines the control samples as undamaged and determines a lesion frequency in experimental samples based on any decrease in amplification efficiency relative to the control samples [107]. One nuclear genome target (9,3 kb) and one mitochondrial genome target (10,9 kb) were amplified. The DNA damage assay is able to quantitatively measure the number of polymerase-stalling lesions based on the amount of amplification obtained from the QPCR [105, 106, 108]. To calculate DNA copy number we utilized a real-time PCR assay in which by using a standard the actual DNA content can be

calculate [109, 110]. This method is particularly advantageous because the standard curve is run along with the samples and the actual number of copies can be calculated.

Phenotype-based screening to identify disease suppressors

The screen was run in 12-well plates. Each well contained: 2 ml solid NGM+50 µL UV killed bacteria lawn+50 µl drug solution in final 0.25% DMSO. In each plate 3 wells were used for RNAi without any compound (0.25% DMSO as control) and 3 wells for pL4440 RNAi both to check the efficacy of the RNAi and to have a negative control of animal development on the empty vector (**Figure S5b**). The screening has been repeated for each compound between 1 (in case they gave 0 rescue at the first trial) and 5 times (in case they gave a partial rescue of the arrested development).

Aldicarb-induced paralysis Assay

The time-course for aldicarb-induced paralysis is dependent on the efficacy of synaptic transmission between the neuron and the muscle (i.e., the speed at which an animal becomes paralyzed by aldicarb depends on the worm's ability to secrete acetylcholine). Consequently, this assay can be used to assess synaptic transmission. Mutant worms with a block in neurotransmitter release will have less acetylcholine accumulation in the presence of aldicarb. Therefore, these worms will take longer than the wild type (WT) to become paralyzed by Aldicarb. Conversely, worms that have enhanced neurotransmitter release will have more acetylcholine accumulation in the presence of aldicarb. These worms will become paralyzed more rapidly than the wild type [56]. We used plates containing either 0.5 mM or 1 mM final aldicarb (33386 Sigma-Aldrich) concentration in the NGM. Briefly, the animals were all L2/L3 larvae on one day of the assay; they were grown on RNAi plates before the beginning of the assay when 25/30 worms were transferred on a small spot (4 µl) of OP50 *E. coli* in the center of the agar plate. The small spot concentrates the animals into a small single field of view, thus making it easier for careful examination of all animals on a plate. After placing the animals on to an Aldicarb plate they were left at RT. Every 30 min, for a total of 5.5 hours, the worms were assayed for paralysis. (We define a worm as paralyzed by the absence of movement when prodded three times with a platinum wire on the head and tail).

Levamisole-induced paralysis Assay

Levamisole is another drug that acts at the neuromuscular junction to cause spastic paralysis. Levamisole is a selective agonist of the major subtype of ligand-gated acetylcholine receptors (AChRs) located at the postsynaptic side of the neuromuscular junction, and acts as the major determinant of synaptically evoked muscular contraction, hence the action of levamisole is largely independent of any acute interaction with presynaptic release of acetylcholine. Therefore, whilst the aldicarb assays give an insight into the presynapse and postsynapse combined, the levamisole assays inform only on the postsynapse **[57]**. The levamisole assay was executed in the same manner as the aldicarb assay. We used 50 μM final concentration. The levamisole stock solution (100 mM in $_{dd}H_20$) was added to the liquid NGM. Briefly, the animals were all L2/L3 larvae on one day of the assay. They were grown on RNAi plates before the beginning of the assay when 25/30 worms were transferred on a small (4 μl) spot of OP50 *E. coli* bacteria onto the center of the plate. After placing the animals onto a Levamisole plate they were left at room temperature (RT) and assayed for paralysis every 15 minutes for 3 hours.

(PTZ)-induced paralysis Assay

Pentylenetetrazole (PTZ) is a gamma-aminobutyric acid (GABA) receptor antagonist, which can be employed together with aldicarb to characterize signaling at *C. elegans* neuromuscular junctions (NMJs) and facilitate our understanding of antagonistic neural circuits [58].

PTZ sensitivity assay was executed similarly to the levamisole and aldicarb assay. Briefly, 75 μl of a 100 mg/mL stock solution (in $_{dd}$H20) was added to plates containing 3 mL of solid NGM, making a final concentration of 2,5 mg/ml. The PTZ plates were allowed to dry for roughly 60-120 minutes at RT with the lids open. The animals were all L2/L3 larvae on one day of the assay. They were grown on RNAi plates before the beginning of the assay when 15/17 worms were transferred on a small spot (4 μl) of OP50 *E. coli* onto the center of the agar plate. After placing the animals on to a PTZ plate they were left at RT and scored for head convulsions and full-body paralysis after 30 minutes and at one hour. In this assay, paralyzed worms were not removed from the plate.

Because of PTZ instability the plates were prepared fresh every time shortly before performing the experiment.

The *C. elegans* strain *unc-49*(e407) was used as positive control. This GABAergic mutant shows significantly more anterior convulsion and full-body paralysis compared to wild-type animals (as far as our observations and as described in [111]).

Measurement of ROS levels

Relative quantification of mitochondrial superoxide levels by fluorescence microscopy (with MitoSOX red). Synchronous L3 stage worm populations of each strain was grown on NGM plates spread with RNAi bacteria and 10 µM MitoSOX Red (Molecular Probes, Eugene, OR). After 24-hour incubation, nematodes were transferred to fresh NGM RNAi plates for one hour to clear their guts of residual dye. Living nematodes were paralyzed *in situ* by directly adding 1 mg/ml levamisole to NGM agar plates. Photographs were taken immediately in the dark using a CY3 fluorescence filter. Subsequently, the terminal pharyngeal bulb (PB) was manually circled to quantify the region's mean intensity using ImageJ software.

Quantification of Gene Expression

The effect of *nuo-5* and *lpd-5* silencing and/or lutein treatment on the induction of different transgenic strains was investigated on synchronized population of L3 worms. The nematodes were placed in a 14 µl S-Basal drop on a microscope glass slide, anesthetized with NaN_3 10mM, covered with a cover slide and immediately imaged. Pictures were acquired with an Imager2 Zeiss fluorescence microscope, magnification 10-fold. The images were analyzed as follow:

For the SJ4100 and CL2166 strains the GFP intensity of the total body was quantified (**Figure S3c**). Concerning the JIN1679 strain, for each animal the number of nuclei showing HLH-30 nuclear translocation (between the pharynx and the vulva) (**Figure S3d**) were counted with a macro specifically customized with ImageJ.

With the KP3928 strain the intensity of the fluorescence was quantified in the pharynx, specifically, two circular area where designed with ImageJ corresponding to anterior and posterior pharyngeal bulbs and the GFP intensity was quantified in the two areas (**Figure S12a**).

For $P_{glb\text{-}10}$::GFP the intensity of the neuronal nuclei located in the pharyngeal area was quantified (**Figure S12b**). For the $P_{dct\text{-}1}$::GFP a circular region in the middle body was selected to quantify the GFP signal (**Figure S9d**). For the selection of the area and the quantification of the signal the software ImageJ (http://imagej.nih.gov/ij/) was used.

For the LX929 the intensity of the second proximal head neuron was quantified (**Figure S12c**).

With the vjIs47 strain the intensity of the fluorescence was quantified in neuronal bodies in the pharynx and in the ventral nerve cord (VNC), specifically, for the pharynx two circular area where designed with ImageJ corresponding to anterior and posterior pharyngeal bulbs, for the VNC a rectangular area was designed between the vulva and the tale and the GFP intensity was quantified in the selected areas (**Figure S12d**).

In each experiment a minimum of 15 to 20 animals per condition were used. The graphs represent the mean and the SEM of three independent biological replicates.

RNA extraction and Microarray

Total RNA was extracted according to [112]. Briefly, we carried out the transcriptomic profile of three different aged-matched cohorts of *C. elegans* upon genetic-mediated disruption of mitochondrial function (treated and untreated with Lutein) and compare their fingerprints with that of wild-type animals. Worms at the desired larval stage (L3) were wash off three big agar plates spotted with the RNAi bacteria under study (*nuo-5*, *lpd-5* and pL4440 for control). The plates were supplemented either with 1 µM Lutein or 0.25 % DMSO for control. Individual *C. elegans* were collected into nuclease-free water and frozen at −80 °C until needed. Frozen worm pellets were re-suspended in lysis buffer and the same volume of Stainless steel beads (6.0 mm RNase free) was added. A TissueLyser II (Qiagen) was used with 2 shakes for 2 minutes at 30 Hz. Total RNA was prepared from each sample using the RNeasy Mini Kit and QIAshredder according to the manufacturer's instructions (Qiagen-74104 and 79654). Total RNA from 5 different biological replicas was extracted, on column purified to remove small RNA fractions, and treated with DNAse (RNeasy kit, Quiagen). The RNA was be then processed, cDNA synthesis and quality control, hybridization and Affymetrix *C. elegans* Gene 1.0 ST Microarrays scanning were performed. Those steps were carried out at the Center for Biological and Medical Research (BMFZ), Facility of the Heinrich Heine University of Düsseldorf. Obtained raw data (Affymetrix.cel-files) were pre-processed.

The data showed in **Figure 3** was analyzed using R version 3.5.1 (2018-07-02). The data were RMA normalized by the oligo package and annotated using pd.elegene.1.0.st package [113]. The list of differentially expressed genes (DEG) was obtained using limma package [114] with FDR correction using a cut-off of adjusted p-value<0.05. The list of unfiltered differentially expressed genes was plot as enhanced volcano with cut-off 1 for log2FC and 10^{-6} for P value(**Figure S4c-d**).

The data showed in **Figure 5** was analyzed using Partek Flow (build 7.0.18.1116). The data were RMA normalized and annotated using the STAR module. The list of differentially expressed genes (DEG) was obtained by ANOVA filtering with FDR correction using the GSA module with a cut-off of adjusted p-value<0.05. The list of DEG between *nuo-5* and *nuo-5* lutein treated worms was used to perform unsupervised Euclidian hierarchical clustering. The fold changes are represented as log2FC (base-2 logarithm of the fold change).

Venn diagrams (**Figure 3a** and **5a**) and pathways representative for a selected list of genes were visualized as network plot of enriched terms in **Figure 5c** was created with ClueGO v2.5 [115, 116], and statistical test used was enrichment/depletion (Two-sided hypergeometric test). The correction method used was Bonferroni step down.

The network plots of enriched terms in **Figure 3d-e** and **S10** were created in R, using Bioconductor [117-119]. Specifically, cnetplot function was used to extract the complex association [120]. R version 3.5.1 (2018-07-02), clusterProfiler_3.8.1, enrichplot_1.0.2, Bioconductor version 3.8.

RNA extraction and qPCR

Total RNA extraction was performed as described above for the microarray. In this case only 3 biological replicas (instead of 5) were used to extract the total RNA and the cDNA was synthetized using GoScript™ Reverse Transcription Mix (Promega A2790).

Primer pairs used for the qPCR:

vps-35: 5'-GGAATACGACCGACCAGGAG-3' and 5'-TGCATCCATGGTTTTTCCCTTAT-3';

nlp-40: 5'-GTTGCGGTTTTTGCGGCTC-3' and 5'-ATCCAAGGAATGTGTCGGCT-3';

unc-10: 5'-GGGGAGCAGAAGGGAAAAGA-3' and 5'-CCAAGAGGACCATCAGCGAG-3';

gbf-1: 5'-GGCTCGGAGACAATACCAACT and 5'-ATCGGCAACCTCATTCAGCA;

F53B2.5: 5'-ATGCCATCACCAGTAGCTCG-3' and 5'-AAGCATGTCGATCCGTGTGG;

nuo-5: 5'-TCGAGCCGTTTCTGAGGTTT-3' and 5'-GTGGGGAGCGATCTCATTCA-3';

Reference genes:

eif-3.C: 5'-ACCACTCTGCAAACCGTCAA-3' and 5'ACTCTTGAGTGTCATCCTTCAG-3';

csq-1: 5'-GCCAGGATCAGTTGCTCTCA-3' and 5'-AAGTTGGGGCGAAAAGTGGA-3'.

Synchrotron Fourier Transform Infrared Microspectroscopy (SR-µFTIR)

Eggs were placed on agar plates (with or without lutein) and worms collected at L3 stage (stored at 20ºC). After washing three times with MilliQ water, worms were transferred to CaF_2

windows and dried in vacuum condition. μFTIR experiments were performed at the MIRAS beamline at ALBA synchrotron, using a Hyperion 3000 Microscope coupled to a Vertex 70 spectrometer (Brucker) equipped with 36x magnification objective. The measuring range was 650−4000 cm^{-1} and the spectra collection was done in transmission mode at 4 cm^{-1} spectral resolution. For single point measurements, a mercury cadmium telluride (MCT) detector was used with an aperture dimension of 10 μm × 10 μm and synchrotron light was used co-adding from 128-256 scans. Background spectra were collected from a clean area of each CaF2 window. A focal plane array (FPA) detector was used for imaging measurement using the internal source co-adding 256 scans. FTIR data was analysed using OPUS 7.5 (Brucker), Unscrambler 10.5 and Matlab R2010b (Mathworks). Spectra exhibiting low signal to noise ratio or saturation were deleted. Remaining spectra were corrected for Resonant Mie Scattering by an open-source algorithm provided by Gardner group [121]. Matrigel was used as reference spectrum, 10 iterations, a scattering particle diameter between 2-18 μm and a refractive index 1.1-1.5. A second-order Savitsky-Golay derivative with 9 smoothing points and a polynomial order of two was applied to the corrected data to eliminate baseline effects and improve peak resolution. Lipid oxidation, amide oxidation and lutein ratio were addressed by calculating the absorption ratios for each spectrum, v_s(C=O) 1745 cm^{-1} /v_{as} (CH_2) 2921 cm^{-1} , v_{as} (C=O) 1745 cm^{-1}/v_s(Amide) 1654 cm^{-1} and v(Lutein) 1515 cm^{-1}/v_{as} (CH_2) 2921 cm^{-1}.

Human cells methods

Cells and culture conditions

Primary human skin fibroblasts (NHDF-neo, Lot Nr.: 7F3956; Lonza) were used as control cell line. Cell culture model systems of NDUFS4 and NDUFS1 deficiency included a primary human skin fibroblast cell line from a patient with a homozygous nonsense mutation c.20C>G; p.(Ser7*) in NDUFS4 (NM_002495.2) and a primary human skin fibroblast cell line from a patient with a compound-heterozygous mutation c.1855G>A; c.1669C>T in NDUFS1. All fibroblasts cell lines were cultured in DMEM with GlutaMAX™-I (Gibco by life technologies) supplemented with 10% FBS and 1% penicillin-streptomycin (5,000U/ml). Medium was replaced every 2-3 days and cells were split when the desired confluence (70-90%) had been reached.

Measurement of ROS levels

Specific measurements of mitochondrial ROS levels were performed with some modifications as described before [122]. Briefly, cells were cultured on glass bottom dishes (27 mm; Nunc by Thermo Fisher Scientific) in DMEM with GlutaMAX™-I (low glucose, Gibco by life technologies) supplemented with 10% FBS and 1% penicillin-streptomycin (5,000U/ml). Either lutein (10 µM, 20 µM or 40µM; Sigma) or vehicle (0,1%, 0,2% or 0,4% dimethyl sulfoxide, DMSO, Sigma) was added to the culture medium and cells were cultured for 24 h, 48 h and 72 h in a humidified atmosphere (95% air, 5% CO2) at 37°C.

Next, cells were incubated with MitoSOX ™ Red (5 µM, 10 min, 37°C; Invitrogen). The red fluorescence was documented using an Axio Observer Z1 microscope (Zeiss) with the dehydroethidium filter set (F39-500, F48-515, F47-895; AHF Analysetechnik). Images were analysed and fluorescence intensity was quantified using ImageJ software (Wayne Rasband at the National Institutes of Health; http://rsbweb.nih.gov/ij/).

Statistical Analysis

Data are represented as mean ± SEM from at least three independent biological replica carried out in a blinded manner where possible. Statistical analyses were performed using either two-sided Student's t-test, one-way ANOVA for multiple comparisons, or two-way ANOVA followed by Tukey's multiple-comparisons test for multiple comparisons and time-points. GraphPad Prism 6 software was used for all statistical analysis to calculate significance as follows: *p = 0.01 to 0.05, **p = 0.001 to 0.01, ***p = 0.0001 to 0.001, and ****p < 0.0001 versus respective control conditions.

5 Acknowledgment

We thank Prof. Dr. Peter Proksch at the Heinrich Heine University of Duesseldorf for providing us with the compound library used in the suppressor screening, Núria Benseny-Cases at the MIRAS beamline in ALBA Synchrotron Light Source, Cerdanyola del Vallès in Barcelona and Genis Rabost for their assistance with the FTIR measurements and analysis. We also thank Anthony Luz for his assistance in using the Seahorse XFe24 Analyzer with *C. elegans* as well as for sharing the protocols, and Ian Ryde for his support with the DNA damage assays. Finally, we

thank the Caenorhabditis Genetics Center (funded by the National Institutes of Health Office of Research Infrastructure Programs: P40OD010440) for strains and also D. Sieburth and J. Kaplan for providing additional strains used in this work. The Wood-Whelan fellowship covered Silvia Maglioni visit costs to Joel N. Meyer Laboratory. This work was possible thanks to financial support to NV from the German Research Foundation (DFG grants VE663-3/1 and VE663/8-1), the Federal Ministry of Education and Research (BMBF/DLR project MiTyrAge), and the Heinrich Heine University of Duesseldorf (Strategic Research Funding 2014). JNM acknowledges funding from the National Institutes of Health (P42ES010356). ZL acknowledges the fellowship from China Scholarship Council (CSC201607030005) and AL acknowledges the financial support from the Spanish Ministry of Science, Innovation and Universities (RTI2018-096273-B-I00) and the 'Severo Ochoa' Programme for Centers of Excellence in R&D (SEV-2015-0496). NR acknowledges the ERC Stg 337327 MitoPexLyso.

6 Author contributions

SM and NV designed the experiments. SM, MM, LZ and VB performed the experiments. SM, NV, MM, LZ, AS, NR analyzed the data. SM and NV wrote the paper. FD, AL, NR, JM edited the manuscript.

7 Declaration of interest

The authors declare no competing interests

8 Data availability

The data that support the findings of this study are available from the corresponding author upon reasonable request. The GEO accession numbers for microarray data reported in this paper are GSE144573 and GSE144574. Cell lines were obtained from patient-derived primary human skin

fibroblasts. Ethical approval and patient consent for their use was obtained. Cell lines are available from the authors upon reasonable request.

9 Figure Legends

Figure 1. Phenotypic screening to identify *C. elegans* models for human mitochondrial-associated disorders.

a) At Day 0 animals were allowed to lay eggs on undiluted bacteria expressing dsRNA for each clone under study. Progeny development was observed for the following 3/4 days (P0 or parental generation). Three possible scenarios were then identified for the different RNAi clones. 1) No effect (black): worms reached adulthood in 3 days and looked similar to wild-type, control (empty-vector) treated worms. These clones were not subsequently followed. ii) A "mild" phenotype (light blue): decreased size and fertility and slow development were observed. iii) A "strong" phenotype (dark blue): sterility, growth arrest or lethality were observed. The clones giving a "mild" phenotype were followed in the next generation, in search of a strong effect (Day 6/7, F1 or first filial generation). If a strong phenotype was instead observed in the P0 then the RNAi bacteria were diluted with bacteria expressing empty vector (1:10 or 1:50), an egg lay was performed and the progeny was followed again in the P0 to identify a mild effect.

b-c) Representative pictures of different phenotypes induced by mild (P1 or Diluted) or strong (F1 or undiluted) gene suppression after 4 days from egg-lay. Pictures were acquired with a Leica MZ10 F modular stereo microscope connected to a color digital camera. Scale Bars 500 µm.

Figure 2. Severe suppression of Complex I genes significantly impairs sensory neurons and mitochondrial functionality

Animals were fed bacteria transformed either with empty-vector (con) or with vector expressing dsRNA against *nuo-5* or *lpd-5*. **a-b**) Chemotaxis index reached after 240 minutes in response to 1% Butanol or 1% Pyrazine respectively. N=3, n=100-250 per group. **c-f**) Basal OCR, maximal OCR and ATP-linked OCR were measured using the Seahorse XF24 Analyzer while ATP production was measured using the luciferase-expressing strain PE255. N=3, n=1000-1500. **g**) ROS production was measured with MitoSOX Red. N=2, n=20-25. **h**) Lipid oxidation assessed with SR-µFTIR. N=3, n=15-20. **i**) $P_{gst\text{-}4}$::GFP expression, N=4, n=10-20. **j**) $P_{hsp\text{-}6}$::GFP expression. N=4, n=15-20. **k**) $P_{dct\text{-}1}$::DCT-1::GFP expression. N=2, n=15-25. **l**) $P_{hlh\text{-}30}$::HLH-30::GFP expression. N=4, n=10-20. In all panels asterisks (*) denote statistical significance. *p-

value <0.05 **p-value < 0.01, ***p-value < 0.001 ****p-value < 0.0001. Bar graphs represent means ± SEM**.** One-way ANOVA. N, number of trials. n, number of animals.

Figure 3. Mild and strong suppression of *nuo-5* lead to different gene expression profiles. a) Venn diagram of the differentially altered genes identified in the microarray analysis. The transcriptomic profile in control L3 larvae was compared with that of mild or strong (arrested) *nuo-5* RNAi. **b**) GO analysis of the 303 uniquely altered genes between mild vs strong *nuo-5* RNAi and **c**) of the 1152 genes uniquely altered between strong *nuo-5* RNAi vs control. **d**) Network plot of enriched terms between strong *nuo-5* RNAi vs control and **e**) for mild vs strong *nuo-5* RNAi were created in R, using Bioconductor. For statistical analysis Enrichment/Depletion, two-sided hypergeometric test was used followed by correction with Bonferroni step down.

Figure 4. Phenotype-based screening identifies lutein ability to rescues behavioral and cellular defects in models of Human Complex I deficiency

a-b) Compounds rescuing more than 20% of the population. **a**) *p-value 0.0379 and ****p-value < 0.0001 compared to *nuo-5* RNAi in DMSO **b**) *p-value 0.022, **p-value 0.001, ****p-value < 0.0001 compared to *lpd-5* RNAi DMSO (N=2-4, n= 40). **c**) Representative pictures of 4 wells of a 12-well plate 3 days after eggs hatching. Scale bars, 1 mm. **d,f**) Chemotaxis curves and **e,g**) maximum chemotaxis index, reached after 240 minutes using as attractants **d,e**) 1 µl of 1% pyrazine or **f,g**)1 µl of 1% butanol. N=3, n=100-250, two-way ANOVA followed by Tukey's multiple-comparisons test. **h**) ROS production, measured with MitoSOX Red, quantified in the pharyngeal bulb. N=2, n=20-25. **i**) ROS production in patients' derived skin fibroblasts after 24 hours incubation with lutein. N=3. **j**) Quantification of GFP nuclear translocation in a strain expressing the $P_{hlh\text{-}30}$::HLH-30::GFP transgene. N=4, n=10-20. In **d**, **e**, **f**, **g**, **h** and **j** animals were fed bacteria transformed either with empty-vector (con) or with vector expressing dsRNA against *nuo-5* or *lpd-5* treated with lutein 1 µM (unless otherwise specified) or left untreated. Bar graphs represent means ± SEM. Asterisks (*) denote significant differences vs control, # denote differences among conditions. One-way ANOVA unless otherwise indicated. *p-value <0.05 ** p value < 0.01, ***p-value < 0.001, ****p-value < 0.0001.

Figure 5. Microarray analysis of worms treated with bacteria expressing empty-vector control, or strong RNAi against *nuo-5* or *nuo-5* treated with lutein.

a) Venn diagram obtained using the online tool: http://bioinformatics.psb.ugent.be/webtools/Venn/.

b) Unsupervised hierarchical clustering of the transcripts corrected by treatment of the mutant *nuo-5* with 1 µM lutein. Each of the twelve lines represents a sample, and each of the columns represents a transcript. Expression levels (log2FC) are represented by a heatmap (the scale is included in the top-right quadrant, green represents down-regulation, min log2FC= -2.39; red represents up-regulation, max log2FC= 3.13).

The microarray data were obtained with a total of 16 *C. elegans* samples. The analysis included the 143 genes significantly differentially expressed between *nuo-5* vs *nuo-5* + lutein (light blue circle in the Venn diagram in panel (**a**). **c**) Pathways enriched in the microarray *nuo-5* vs *nuo-5* + lutein designed using ClueGO v2.5.

Figure 6. Lutein suppresses an *nlg-1*-dependent synaptic defect in *nuo-5*-depleted animals.

In all panels strains were fed bacteria transformed either with empty-vector (con, black bars) or with vector expressing dsRNA against *nuo-5* (light blue bars) and left untreated or treated with 1□M Lutein. Bar graphs represent means ± SEM. Asterisks (*) denote significant differences vs control, # denote differences among conditions. *p-value <0.05 ** p value < 0.01, ***p-value < 0.001, ****p-value < 0.0001. One-way ANOVA unless otherwise indicated. **a**) Bars indicate percentage of animals paralyzed after 180 minutes on plates containing 0.5 mM aldicarb. N=3, n=25-30. **b**) Bars indicate percentage of animals paralyzed on plates containing 50 µM Levamisole. N=4, n=25-30. **c**) Bars indicate percentage of animals with the indicated phenotypes after 1 hour of exposure to 2.5 mg/ml PTZ. N=4, n=15-17. Asterisks denote the differences only of the full body-paralysis phenotype. **d-g**) Quantification of GFP expression in the indicated transgenic strains. N=3, n=20-35. **h**) Frequency of body bends in liquid media ("thrashing") were quantified manually for one minute. N=3, n=15. **i**) Bars indicate the mean survival in minutes on plates containing 0.5 mM aldicarb. N=3, n=25-30. **j**) Bars indicate mean survival on plates containing 50 µM Levamisole. N=4, n=25-30. **k**) Bars indicate the percentage of animals showing full-body paralysis after one hour of exposure to 2.5 mg/ml PTZ. N=4, n=15-17. **l**) Bars indicate the percentage of different developmental stages in wild-type and *nlg-1* mutants after 6 days from egg lay. Asterisks denote differences between the percentages of animals which

reached the gravid adult (GA) stage. N=4, n=40, two-way ANOVA, followed by Tukey's multiple-comparisons test.

Figure 7. Graphical abstract summarizing major results.

According to our findings, *nuo-5*-depleted animals display an altered functionality of the cholinergic synapses. Specifically, compared to **a)** wild-type animals, **b)** *nuo-5* deficient worms present excessive synaptic excitation, likely due to an enhanced ACh buildup in the synaptic cleft (as a result of a defective negative feedback) leading to hypersensitivity to aldicarb, levamisole, and PTZ. Similar to the disease state these animals also present with development and motor-sensory defects when compared to control nematodes. **c)** Treatment from eggs with 1 µM lutein rescues most of these defects. These findings, together with animals' gene expression profile and data in the literature, lead us to hypothesize that lutein could act either by directly binding the cell-adhesion pre-synaptic protein, NLG-1, and/or by inhibiting the enzyme AChE, and/or by modulating intracellular recycling/trafficking pathways. Regardless from its mode of action, its effect is to reinstate normal levels of ACh at the NMJ thus restoring the retrograde inhibition of ACh release.

10 Tables

Table I

Cosmid ID	Gene	Human ortholog, Short gene description	Disease	RNAi Power	Phenotype
ZK973.10	*lpd-5*	NDUFS4, NADH-Dehydrogenase, Fe-S protein complex I subunit	Complex I deficiency (Leigh Syndrome)	mild	few progeny
				strong	slow development; few eggs
Y45G12B.1	*nuo-5*	NDUFS1, NADH-Ubiquinone Oxidoreductase Fe-S Protein 1; complex I	Complex I deficiency (Leigh Syndrome)	mild	pale, small, few eggs
				strong	slow development, arrested L2/L3

C09H10.3	***nuo-1****	NDUFV1, mitochondrial NADH Dehydrogenase Ubiquinone Flavoprotein 1	Complex I deficiency (Leigh Syndrome)	mild	pale, thin, sterile
				strong	arrested as L2/L3
T20H4.5	**T20H4.5***	NDUFS8, ubiquinone oxidoreductase core subunit S8	Complex I deficiency (Leigh Syndrome)	mild	pale, thin, small, few eggs
				strong	arrested L2/L3
F53F4.10	**F53F4.10**	NDUFV2, Fe-S complex I	Complex I deficiency Parkinson's Disease Susceptibility	mild	slow development
				strong	slow development, arrested L2/L3
C01F1.2	***sco-1***	SCO-1, SCO cytochrome c oxidase assembly protein 1	Cytochrome-c oxidase deficiency disease.	mild	
				strong	slow development, sick, thin, sterile
H14A12.2	***fum-1***	FH, fumarate hydratase, predicted to have fumarate hydratase activity	Fumarase deficiency, Leigh Syndrome	mild	few eggs
				strong	few progeny, slow development
T12E12.4	***drp-1***	DNM1L (dynamin 1 like)	Optic Distrophy	mild	
				strong	small, pale
D2013.5	***eat-3****	OPA-1 or *mgm*-1, dynamin family GTPase	Dominant Optic Atrophy	mild	thin
				strong	thin, slow development
F54H12.1	***aco-2***	ACO2, Mitochondrial aconitase	Infantile Cerebellar-Retinal Degeneration and Optic Atrophy 9	mild	few progeny
				strong	sterile
Y47G6A.10	***spg-7****	AFG3L2, AFG3 like matrix AAA peptidase subunit 2	Spinocerebellar ataxia (SCA28)	mild	pale, small, thin few eggs, few progeny
				strong	slow development, arrested L2
F23B12.5	***dlat-1****	DLD, dihydrolipamide deidrogenase	Lactic Acidosis	mild	sterile, slow moving
				strong	
K08E3.7	***pdr-1****	PARK-2 or parkin, E3	Parkinson's	mild	slow moving, pale, few

		ubiquitine ligase	Disease		progeny
				strong	slow moving, pale, few eggs, protruding vulva
F25B4.6	***hmgs-1****	HMGCS1 & HMGCS2, 3-hydroxy-3-methylglutaryl-CoA synthase 1 & 2	Mitochondrial HMG-CoA Synthase Deficiency	mild	pale, thin, slow moving
				strong	sick, pale, slow moving
C15F1.7	***sod-1***	SOD-1, Cu-Zn SOD1	Amyotrophic lateral sclerosis	mild	small
				strong	
T22B11.5	***ogdh-1***	OGDH, predicted to have oxoglutarate dehydrogenase (succinyl-transferring) activity	Alpha ketoglutarate deficiency	mild	thin, pale, sterile adults
				strong	thin, pale, slow development, sick
W02F12.5	***dlst-1****	DLST, dihydrolipoamide S-succinyltransferase	Possible cause of familial Alzheimer's disease	mild	Skinny, pale
				strong	long, pale
Y46G5A.2	***cox-10***	COX10, complex IV farnesyl transferase	Mitochondrial complex IV deficiency	mild	few eggs, pale
				strong	
T27E9.1	***tag-61****	SLC25A5, solute carrier family 25 member 5, mitochondrial adenine nucleotide transporters	Mitochondrial Phosphate Carrier Deficiency	mild	thin, pale
				strong	small, pale, sterile, protruding vulva
F01F1.12	**aldo-2**	ALDOB, encodes a fructose-bisphosphate aldolase	Hereditary fructose intolerance	mild	pale
				strong	sick, pale

Table legend

* These clones showed a strong phenotype already in the parental generation (P0, see Figure 1) when used undiluted, and the mild effect was thus achieved by diluting the dsRNA expressing bacteria (P0, 1/10 or 1/15). Lifespan for these clones were carried out accordingly in the parental generation (P0) left undiluted or diluted (Table SI). For all the other clones a mild phenotype was observed in the undiluted parental generation (P0), while a strong one in the first filius generation (F1). Accordingly, lifespan with these clones were completed with P0 & F1on undiluted dsRNA expressing bacteria (Table SII).

Genes in red are complex I genes giving a typical *Mit* mutants phenotype in our first screen, which we mainly followed up on.

11 References

1. Kwong, J.Q., M.F. Beal, and G. Manfredi, *The role of mitochondria in inherited neurodegenerative diseases.* J Neurochem, 2006. **97**(6): p. 1659-75.
2. Wallace, D.C., *A mitochondrial paradigm of metabolic and degenerative diseases, aging, and cancer: a dawn for evolutionary medicine.* Annu Rev Genet, 2005. **39**: p. 359-407.
3. Koopman, W.J., et al., *Mammalian mitochondrial complex I: biogenesis, regulation, and reactive oxygen species generation.* Antioxid Redox Signal, 2010. **12**(12): p. 1431-70.
4. Distelmaier, F., et al., *Mitochondrial complex I deficiency: from organelle dysfunction to clinical disease.* Brain, 2009. **132**(Pt 4): p. 833-42.
5. Chinnery, P.F., *Mitochondrial Disorders Overview*, in *GeneReviews(R)*, R.A. Pagon, et al., Editors. 2014: Seattle (WA).
6. Baertling, F., et al., *A guide to diagnosis and treatment of Leigh syndrome.* J Neurol Neurosurg Psychiatry, 2014. **85**(3): p. 257-65.
7. Silverman, G.A., et al., *Modeling molecular and cellular aspects of human disease using the nematode Caenorhabditis elegans.* Pediatr Res, 2009. **65**(1): p. 10-8.
8. Ventura, N., S.L. Rea, and R. Testi, *Long-lived C. elegans mitochondrial mutants as a model for human mitochondrial-associated diseases.* Exp Gerontol, 2006. **41**(10): p. 974-91.
9. Link, C.D., *C. elegans models of age-associated neurodegenerative diseases: lessons from transgenic worm models of Alzheimer's disease.* Exp Gerontol, 2006. **41**(10): p. 1007-13.
10. Artal-Sanz, M., L. de Jong, and N. Tavernarakis, *Caenorhabditis elegans: a versatile platform for drug discovery.* Biotechnol J, 2006. **1**(12): p. 1405-18.
11. O'Reilly, L.P., et al., *C. elegans in high-throughput drug discovery.* Adv Drug Deliv Rev, 2014. **69-70**: p. 247-53.
12. Maglioni, S., N. Arsalan, and N. Ventura, *C. elegans screening strategies to identify pro-longevity interventions.* Mech Ageing Dev, 2016. **157**: p. 60-69.
13. Lublin, A.L. and C.D. Link, *Alzheimer's disease drug discovery: in vivo screening using Caenorhabditis elegans as a model for beta-amyloid peptide-induced toxicity.* Drug Discov Today Technol, 2013. **10**(1): p. e115-9.
14. Alexander, A.G., V. Marfil, and C. Li, *Use of Caenorhabditis elegans as a model to study Alzheimer's disease and other neurodegenerative diseases.* Front Genet, 2014. **5**: p. 279.
15. Teschendorf, D. and C.D. Link, *What have worm models told us about the mechanisms of neuronal dysfunction in human neurodegenerative diseases?* Mol Neurodegener, 2009. **4**: p. 38.
16. Helmcke, K.J., D.S. Avila, and M. Aschner, *Utility of Caenorhabditis elegans in high throughput neurotoxicological research.* Neurotoxicol Teratol, 2010. **32**(1): p. 62-7.
17. Maglioni, S. and N. Ventura, *C. elegans as a model organism for human mitochondrial associated disorders.* Mitochondrion, 2016.
18. Ventura, N., et al., *Reduced expression of frataxin extends the lifespan of Caenorhabditis elegans.* Aging Cell, 2005. **4**(2): p. 109-12.
19. Zhou, S., Z. Wang, and J.E. Klaunig, *Caenorhabditis elegans neuron degeneration and mitochondrial suppression caused by selected environmental chemicals.* Int J Biochem Mol Biol, 2013. **4**(4): p. 191-200.
20. Wolozin, B., et al., *Watching worms whither: modeling neurodegeneration in C. elegans.* Prog Mol Biol Transl Sci, 2011. **100**: p. 499-514.
21. Rea, S.L., N. Ventura, and T.E. Johnson, *Relationship between mitochondrial electron transport chain dysfunction, development, and life extension in Caenorhabditis elegans.* PLoS Biol, 2007. **5**(10): p. e259.

22. Ventura, N. and S.L. Rea, *Caenorhabditis elegans mitochondrial mutants as an investigative tool to study human neurodegenerative diseases associated with mitochondrial dysfunction.* Biotechnol J, 2007. **2**(5): p. 584-95.
23. Ventura, N., et al., *p53/CEP-1 increases or decreases lifespan, depending on level of mitochondrial bioenergetic stress.* Aging Cell, 2009. **8**(4): p. 380-93.
24. Maglioni, S., et al., *Mitochondrial bioenergetic changes during development as an indicator of C. elegans health-span.* Aging (Albany NY), 2019. **11**(16): p. 6535-6554.
25. Hart, A.C. and M.Y. Chao, *From Odors to Behaviors in Caenorhabditis elegans*, in *The Neurobiology of Olfaction*, A. Menini, Editor. 2010: Boca Raton (FL).
26. Hart, A.C., *Behavior* in *WormBook, The C. elegans Research Community*. 2006.
27. Chalfie, M. and J. Sulston, *Developmental genetics of the mechanosensory neurons of Caenorhabditis elegans.* Dev Biol, 1981. **82**(2): p. 358-70.
28. Sulston, J., M. Dew, and S. Brenner, *Dopaminergic neurons in the nematode Caenorhabditis elegans.* J Comp Neurol, 1975. **163**(2): p. 215-26.
29. Maglioni, S., et al., *Mitochondrial stress extends lifespan in C. elegans through neuronal hormesis.* Exp Gerontol, 2014. **56**: p. 89-98.
30. Gorman, G.S., et al., *Perceived fatigue is highly prevalent and debilitating in patients with mitochondrial disease.* Neuromuscul Disord, 2015. **25**(7): p. 563-6.
31. Matthies, D.S., et al., *The Caenorhabditis elegans choline transporter CHO-1 sustains acetylcholine synthesis and motor function in an activity-dependent manner.* J Neurosci, 2006. **26**(23): p. 6200-12.
32. Luz, A.L., et al., *Seahorse Xfe 24 Extracellular Flux Analyzer-Based Analysis of Cellular Respiration in Caenorhabditis elegans.* Curr Protoc Toxicol, 2015. **66**: p. 25 7 1-15.
33. Meyer, J.N., et al., *Mitochondria as a target of environmental toxicants.* Toxicol Sci, 2013. **134**(1): p. 1-17.
34. Meyer, J.N., T.C. Leuthner, and A.L. Luz, *Mitochondrial fusion, fission, and mitochondrial toxicity.* Toxicology, 2017. **391**: p. 42-53.
35. Yoneda, T., et al., *Compartment-specific perturbation of protein handling activates genes encoding mitochondrial chaperones.* Journal of cell science, 2004. **117**(Pt 18): p. 4055-66.
36. Zysk, J.R., et al., *In vitro binding of a radio-labeled positive allosteric modulator for metabotropic glutamate receptor subtype 5.* Synapse, 2013. **67**(3): p. 135-44.
37. Schiavi, A., et al., *Autophagy induction extends lifespan and reduces lipid content in response to frataxin silencing in C. elegans.* Exp Gerontol, 2013. **48**(2): p. 191-201.
38. Liu, Y., et al., *Caenorhabditis elegans pathways that surveil and defend mitochondria.* Nature, 2014. **508**(7496): p. 406-10.
39. Lapierre, L.R., et al., *The TFEB orthologue HLH-30 regulates autophagy and modulates longevity in Caenorhabditis elegans.* Nat Commun, 2013. **4**: p. 2267.
40. Visvikis, O., et al., *Innate host defense requires TFEB-mediated transcription of cytoprotective and antimicrobial genes.* Immunity, 2014. **40**(6): p. 896-909.
41. Cristina, D., et al., *A regulated response to impaired respiration slows behavioral rates and increases lifespan in Caenorhabditis elegans.* PLoS Genet, 2009. **5**(4): p. e1000450.
42. Falk, M.J., et al., *Metabolic pathway profiling of mitochondrial respiratory chain mutants in C. elegans.* Mol Genet Metab, 2008. **93**(4): p. 388-97.
43. Baruah, A., et al., *CEP-1, the Caenorhabditis elegans p53 homolog, mediates opposing longevity outcomes in mitochondrial electron transport chain mutants.* PLoS Genet, 2014. **10**(2): p. e1004097.
44. Yee, C., W. Yang, and S. Hekimi, *The intrinsic apoptosis pathway mediates the pro-longevity response to mitochondrial ROS in C. elegans.* Cell, 2014. **157**(4): p. 897-909.

45. Maglioni, S., et al., *An automated phenotype-based microscopy screen to identify pro-longevity interventions acting through mitochondria in C. elegans.* Biochim Biophys Acta, 2015. **1847**(11): p. 1469-78.
46. Andreux, P.A., et al., *A method to identify and validate mitochondrial modulators using mammalian cells and the worm C. elegans.* Sci Rep, 2014. **4**: p. 5285.
47. *Carotenoids. Volume 1B: Spectroscopy*. 1995, Basel: Birkhäuser Verlag AG. xvi + 360 pp.
48. Santocono, M., et al., *Influence of astaxanthin, zeaxanthin and lutein on DNA damage and repair in UVA-irradiated cells.* J Photochem Photobiol B, 2006. **85**(3): p. 205-15.
49. Swanson HM, S.J., Gong X, Rubin LP, *Lutein, but not other carotenoids, selectively inhibits breast cancer cell growth through several molecular mechanisms.* FASEB J, 2016: p. 30(1 Suppl):34.2.
50. Liu, R., et al., *Lutein and zeaxanthin supplementation and association with visual function in age-related macular degeneration.* Invest Ophthalmol Vis Sci, 2014. **56**(1): p. 252-8.
51. Kiko, T., et al., *Significance of lutein in red blood cells of Alzheimer's disease patients.* J Alzheimers Dis, 2012. **28**(3): p. 593-600.
52. Xue, C., et al., *Management of Ocular Diseases Using Lutein and Zeaxanthin: What Have We Learned from Experimental Animal Studies?* J Ophthalmol, 2015. **2015**: p. 523027.
53. Sujak, A., et al., *Lutein and zeaxanthin as protectors of lipid membranes against oxidative damage: the structural aspects.* Arch Biochem Biophys, 1999. **371**(2): p. 301-7.
54. Gammone, M.A., G. Riccioni, and N. D'Orazio, *Carotenoids: potential allies of cardiovascular health?* Food Nutr Res, 2015. **59**: p. 26762.
55. Oh, K.H. and H. Kim, *Aldicarb-induced Paralysis Assay to Determine Defects in Synaptic Transmission in Caenorhabditis elegans.* Bio Protoc, 2017. **7**(14).
56. Mahoney, T.R., S. Luo, and M.L. Nonet, *Analysis of synaptic transmission in Caenorhabditis elegans using an aldicarb-sensitivity assay.* Nat Protoc, 2006. **1**(4): p. 1772-7.
57. Mulcahy, B., L. Holden-Dye, and V. O'Connor, *Pharmacological assays reveal age-related changes in synaptic transmission at the Caenorhabditis elegans neuromuscular junction that are modified by reduced insulin signalling.* J Exp Biol, 2013. **216**(Pt 3): p. 492-501.
58. Locke, C., et al., *Paradigms for pharmacological characterization of C. elegans synaptic transmission mutants.* J Vis Exp, 2008(18).
59. Thapliyal, S. and K. Babu, *Pentylenetetrazole (PTZ)-induced Convulsion Assay to Determine GABAergic Defects in Caenorhabditis elegans.* Bio Protoc, 2018. **8**(17).
60. Fleming, J.T., et al., *Caenorhabditis elegans levamisole resistance genes lev-1, unc-29, and unc-38 encode functional nicotinic acetylcholine receptor subunits.* J Neurosci, 1997. **17**(15): p. 5843-57.
61. Lemons, M.L., *An Inquiry-Based Approach to Study the Synapse: Student-Driven Experiments Using C. elegans.* J Undergrad Neurosci Educ, 2016. **15**(1): p. A44-A55.
62. Sieburth, D., et al., *Systematic analysis of genes required for synapse structure and function.* Nature, 2005. **436**(7050): p. 510-7.
63. Meissner, B., et al., *Determining the sub-cellular localization of proteins within Caenorhabditis elegans body wall muscle.* PLoS One, 2011. **6**(5): p. e19937.
64. Hu, Z., et al., *Neurexin and neuroligin mediate retrograde synaptic inhibition in C. elegans.* Science, 2012. **337**(6097): p. 980-4.
65. Staab, T.A., et al., *Regulation of synaptic nlg-1/neuroligin abundance by the skn-1/Nrf stress response pathway protects against oxidative stress.* PLoS Genet, 2014. **10**(1): p. e1004100.
66. Dell'agnello, C., et al., *Increased longevity and refractoriness to Ca(2+)-dependent neurodegeneration in Surf1 knockout mice.* Hum Mol Genet, 2007. **16**(4): p. 431-44.
67. Agostino, A., et al., *Constitutive knockout of Surf1 is associated with high embryonic lethality, mitochondrial disease and cytochrome c oxidase deficiency in mice.* Hum Mol Genet, 2003. **12**(4): p. 399-413.

68. Ingraham, C.A., et al., *NDUFS4: creation of a mouse model mimicking a Complex I disorder.* Mitochondrion, 2009. **9**(3): p. 204-10.
69. Breuer, M.E., et al., *Cellular and animal models for mitochondrial complex I deficiency: a focus on the NDUFS4 subunit.* IUBMB Life, 2013. **65**(3): p. 202-8.
70. Dillin, A., et al., *Rates of behavior and aging specified by mitochondrial function during development.* Science, 2002. **298**(5602): p. 2398-401.
71. Ristow, M. and K. Schmeisser, *Mitohormesis: Promoting Health and Lifespan by Increased Levels of Reactive Oxygen Species (ROS).* Dose Response, 2014. **12**(2): p. 288-341.
72. Luz, A.L., et al., *Deficiencies in mitochondrial dynamics sensitize Caenorhabditis elegans to arsenite and other mitochondrial toxicants by reducing mitochondrial adaptability.* Toxicology, 2017. **387**: p. 81-94.
73. Muraresku, C.C., E.M. McCormick, and M.J. Falk, *Mitochondrial Disease: Advances in clinical diagnosis, management, therapeutic development, and preventative strategies.* Curr Genet Med Rep, 2018. **6**(2): p. 62-72.
74. Devine, M.J. and J.T. Kittler, *Mitochondria at the neuronal presynapse in health and disease.* Nat Rev Neurosci, 2018. **19**(2): p. 63-80.
75. Vos, M., E. Lauwers, and P. Verstreken, *Synaptic mitochondria in synaptic transmission and organization of vesicle pools in health and disease.* Front Synaptic Neurosci, 2010. **2**: p. 139.
76. Jeanneteau, F. and M. Arango-Lievano, *Linking Mitochondria to Synapses: New Insights for Stress-Related Neuropsychiatric Disorders.* Neural Plast, 2016. **2016**: p. 3985063.
77. Nikoletopoulou, V. and N. Tavernarakis, *Regulation and Roles of Autophagy at Synapses.* Trends Cell Biol, 2018. **28**(8): p. 646-661.
78. Birdsall, V. and C.L. Waites, *Autophagy at the synapse.* Neurosci Lett, 2019. **697**: p. 24-28.
79. Schiavi, A., et al., *Iron-Starvation-Induced Mitophagy Mediates Lifespan Extension upon Mitochondrial Stress in C. elegans.* Curr Biol, 2015. **25**(14): p. 1810-22.
80. Stan, A., et al., *Essential cooperation of N-cadherin and neuroligin-1 in the transsynaptic control of vesicle accumulation.* Proc Natl Acad Sci U S A, 2010. **107**(24): p. 11116-21.
81. Calahorro, F. and M. Ruiz-Rubio, *Functional phenotypic rescue of Caenorhabditis elegans neuroligin-deficient mutants by the human and rat NLGN1 genes.* PLoS One, 2012. **7**(6): p. e39277.
82. Matzinger, M., K. Fischhuber, and E.H. Heiss, *Activation of Nrf2 signaling by natural products-can it alleviate diabetes?* Biotechnol Adv, 2018. **36**(6): p. 1738-1767.
83. Hunter, J.W., et al., *Neuroligin-deficient mutants of C. elegans have sensory processing deficits and are hypersensitive to oxidative stress and mercury toxicity.* Dis Model Mech, 2010. **3**(5-6): p. 366-76.
84. Geiss, J.M.T., et al., *Oral administration of lutein attenuates ethanol-induced memory deficit in rats by restoration of acetylcholinesterase activity.* Physiol Behav, 2019. **204**: p. 121-128.
85. Khadija Ghanam, J.D.a.V.J., *Lutein and Zeaxanthin Isomers Inhibit Cholinesterase and Modulate the Expression of Inflammation-Related Genes: In Vitro Models.* International Journal of Ophthalmology and Clinical Research, 2015.
86. Grella Miranda, C., et al., *Influence of nanoencapsulated lutein on acetylcholinesterase activity: In vitro determination, kinetic parameters, and in silico docking simulations.* Food Chem, 2019. **307**: p. 125523.
87. Nolan, J.M., et al., *The impact of supplemental macular carotenoids in Alzheimer's disease: a randomized clinical trial.* J Alzheimers Dis, 2015. **44**(4): p. 1157-69.
88. Desmidt, T., C. Hommet, and V. Camus, *Pharmacological treatments of behavioral and psychological symptoms of dementia in Alzheimer's disease: role of acetylcholinesterase inhibitors and memantine.* Geriatr Psychol Neuropsychiatr Vieil, 2016. **14**(3): p. 300-6.

89. Li, S.Y., et al., *Anti-inflammatory effects of lutein in retinal ischemic/hypoxic injury: in vivo and in vitro studies.* Invest Ophthalmol Vis Sci, 2012. **53**(10): p. 5976-84.
90. Nataraj, J., et al., *Lutein protects dopaminergic neurons against MPTP-induced apoptotic death and motor dysfunction by ameliorating mitochondrial disruption and oxidative stress.* Nutr Neurosci, 2016. **19**(6): p. 237-46.
91. Grella Miranda, C., et al., *Influence of nanoencapsulated lutein on acetylcholinesterase activity: In vitro determination, kinetic parameters, and in silico docking simulations.* Food Chem, 2020. **307**: p. 125523.
92. Arunkumar, R., et al., *Biodegradable Poly (Lactic-co-Glycolic Acid)-Polyethylene Glycol Nanocapsules: An Efficient Carrier for Improved Solubility, Bioavailability, and Anticancer Property of Lutein.* J Pharm Sci, 2015. **104**(6): p. 2085-2093.
93. Kamil, A., et al., *Bioavailability and biodistribution of nanodelivered lutein.* Food Chem, 2016. **192**: p. 915-23.
94. Andreux, P.A., R.H. Houtkooper, and J. Auwerx, *Pharmacological approaches to restore mitochondrial function.* Nat Rev Drug Discov, 2013. **12**(6): p. 465-83.
95. Jansen-Olesen, I., P. Tfelt-Hansen, and J. Olesen, *Animal migraine models for drug development: status and future perspectives.* CNS Drugs, 2013. **27**(12): p. 1049-68.
96. Stiernagle, T., *Maintenance of C. elegans.* WormBook, 2006: p. 1-11.
97. Kamath, R.S. and J. Ahringer, *Genome-wide RNAi screening in Caenorhabditis elegans.* Methods, 2003. **30**(4): p. 313-21.
98. Pierce-Shimomura, J.T., et al., *Genetic analysis of crawling and swimming locomotory patterns in C. elegans.* Proc Natl Acad Sci U S A, 2008. **105**(52): p. 20982-7.
99. Han, S.K., et al., *OASIS 2: online application for survival analysis 2 with features for the analysis of maximal lifespan and healthspan in aging research.* Oncotarget, 2016.
100. Luz, A.L., et al., *Seahorse-based analysis of cellular respiration in Caenorhabditis elegans.* in preparation.
101. Lagido, C., et al., *Bridging the phenotypic gap: real-time assessment of mitochondrial function and metabolism of the nematode Caenorhabditis elegans.* BMC Physiol, 2008. **8**: p. 7.
102. Lagido, C., et al., *Rapid sublethal toxicity assessment using bioluminescent Caenorhabditis elegans, a novel whole-animal metabolic biosensor.* Toxicol Sci, 2009. **109**(1): p. 88-95.
103. McLaggan, D., et al., *Impact of sublethal levels of environmental pollutants found in sewage sludge on a novel Caenorhabditis elegans model biosensor.* PLoS One, 2012. **7**(10): p. e46503.
104. Luz, A.L., et al., *In Vivo Determination of Mitochondrial Function Using Luciferase-Expressing Caenorhabditis elegans: Contribution of Oxidative Phosphorylation, Glycolysis, and Fatty Acid Oxidation to Toxicant-Induced Dysfunction.* Curr Protoc Toxicol, 2016. **69**: p. 25 8 1-25 8 22.
105. Hunter, S.E., et al., *The QPCR assay for analysis of mitochondrial DNA damage, repair, and relative copy number.* Methods, 2010. **51**(4): p. 444-51.
106. Furda, A.M., et al., *Analysis of DNA damage and repair in nuclear and mitochondrial DNA of animal cells using quantitative PCR.* Methods Mol Biol, 2012. **920**: p. 111-32.
107. Meyer, J.N., *QPCR: a tool for analysis of mitochondrial and nuclear DNA damage in ecotoxicology.* Ecotoxicology, 2010. **19**(4): p. 804-11.
108. Furda, A., et al., *Quantitative PCR-based measurement of nuclear and mitochondrial DNA damage and repair in mammalian cells.* Methods Mol Biol, 2014. **1105**: p. 419-37.
109. Rooney, J.P., et al., *PCR based determination of mitochondrial DNA copy number in multiple species.* Methods Mol Biol, 2015. **1241**: p. 23-38.
110. Venegas, V. and M.C. Halberg, *Measurement of mitochondrial DNA copy number.* Methods Mol Biol, 2012. **837**: p. 327-35.
111. Dabbish, N.S. and D.M. Raizen, *GABAergic synaptic plasticity during a developmentally regulated sleep-like state in C. elegans.* J Neurosci, 2011. **31**(44): p. 15932-43.

112. F., H., *Total RNA Extraction from C. elegans.* Bio-protocol Bio101: e47. , 2011.
113. Carvalho, B.S. and R.A. Irizarry, *A framework for oligonucleotide microarray preprocessing.* Bioinformatics, 2010. **26**(19): p. 2363-7.
114. Ritchie, M.E., et al., *limma powers differential expression analyses for RNA-sequencing and microarray studies.* Nucleic Acids Res, 2015. **43**(7): p. e47.
115. Bindea, G., et al., *ClueGO: a Cytoscape plug-in to decipher functionally grouped gene ontology and pathway annotation networks.* Bioinformatics, 2009. **25**(8): p. 1091-3.
116. Bindea, G., J. Galon, and B. Mlecnik, *CluePedia Cytoscape plugin: pathway insights using integrated experimental and in silico data.* Bioinformatics, 2013. **29**(5): p. 661-3.
117. Yu, G., *enrichplot: Visualization of Functional Enrichment Result. R package version 1.0.2.* 2018.
118. Huber, W., et al., *Orchestrating high-throughput genomic analysis with Bioconductor.* Nat Methods, 2015. **12**(2): p. 115-21.
119. Yu, G., et al., *clusterProfiler: an R package for comparing biological themes among gene clusters.* OMICS, 2012. **16**(5): p. 284-7.
120. Team, R.C., *R: A Language and Environment for Statistical Computing*.
121. Bassan, P., et al., *Resonant Mie scattering (RMieS) correction of infrared spectra from highly scattering biological samples.* Analyst, 2010. **135**(2): p. 268-77.
122. Distelmaier, F., et al., *Mitochondrial dysfunction in primary human fibroblasts triggers an adaptive cell survival program that requires AMPK-alpha.* Biochim Biophys Acta, 2015. **1852**(3): p. 529-40.

Figure 1

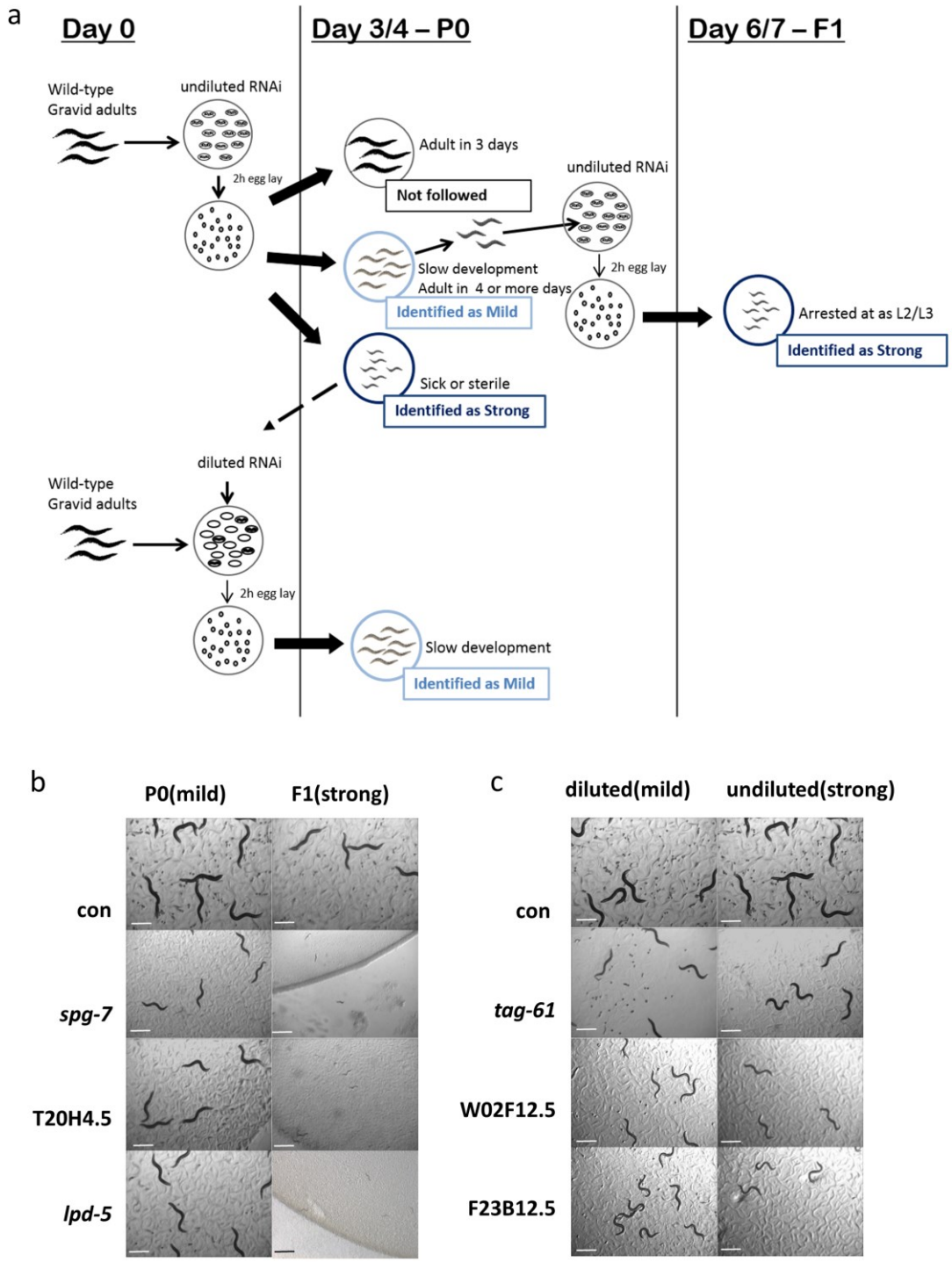
a
Day 0
Day 3/4 – P0
Day 6/7 – F1
Wild-type
Gravid adults
undiluted RNAi
2h egg lay
Adult in 3 days
Not followed
undiluted RNAi
Slow development
Adult in 4 or more days
Identified as Mild
2h egg lay
Arrested at as L2/L3
Identified as Strong
Sick or sterile
Identified as Strong
diluted RNAi
Wild-type
Gravid adults
2h egg lay
Slow development
Identified as Mild
b
P0(mild)
F1(strong)
con
spg-7
T20H4.5
lpd-5
c
diluted(mild)
undiluted(strong)
con
tag-61
W02F12.5
F23B12.5

Figure 2

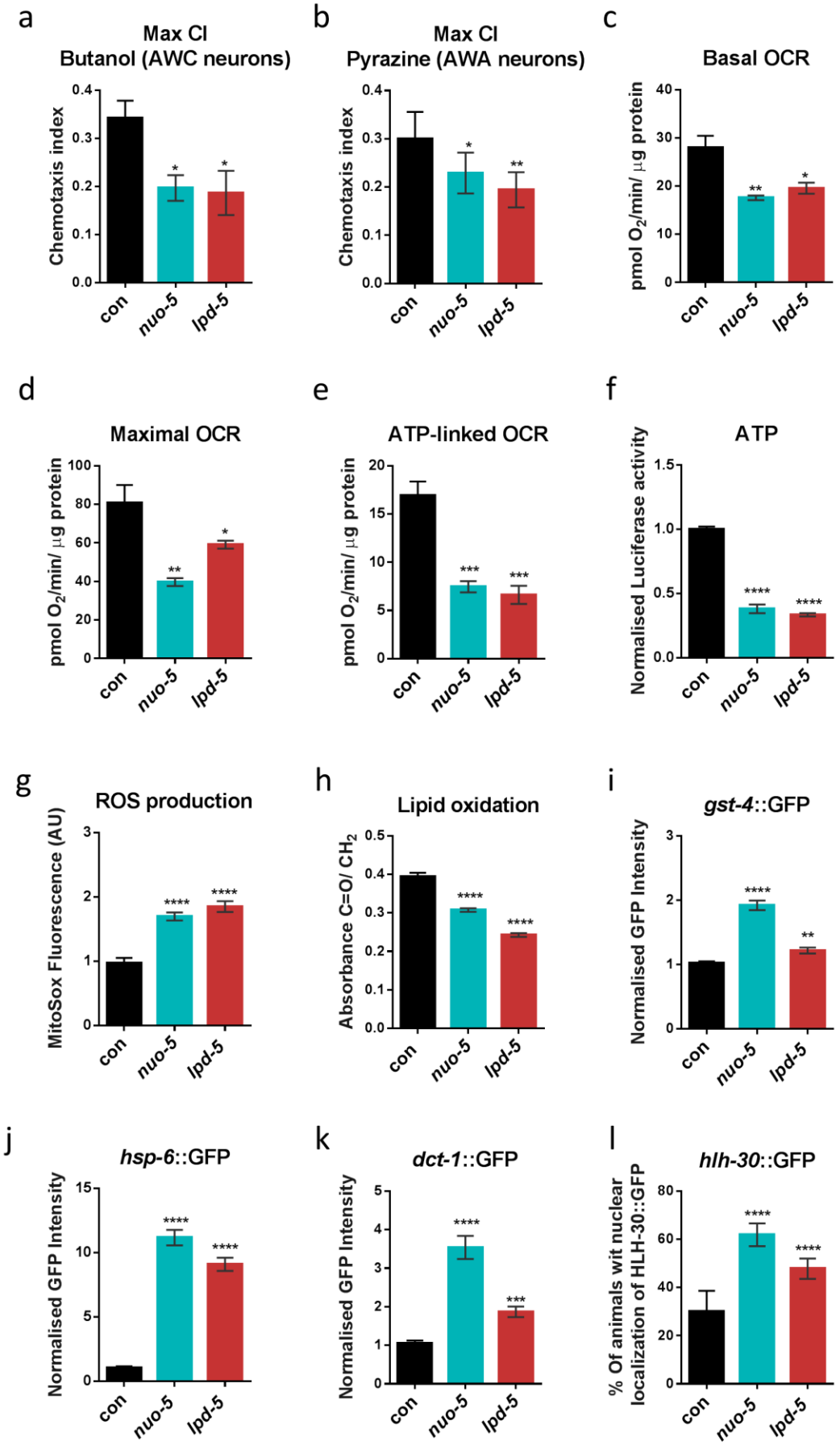
a
Max CI
Butanol (AWC neurons)
Chemotaxis index
0.4
0.3
0.2
0.1
0.0
*
*
con
nuo-5
lpd-5
b
Max CI
Pyrazine (AWA neurons)
Chemotaxis index
0.4
0.3
0.2
0.1
0.0
*
**
con
nuo-5
lpd-5
c
Basal OCR
pmol O2/min/ µg protein
40
30
20
10
0
**
*
con
nuo-5
lpd-5
d
Maximal OCR
pmol O2/min/ µg protein
100
80
60
40
20
0
**
*
con
nuo-5
lpd-5
e
ATP-linked OCR
pmol O2/min/ µg protein
20
15
10
5
0
***
***
con
nuo-5
lpd-5
f
ATP
Normalised Luciferase activity
1.5
1.0
0.5
0.0
****
****
con
nuo-5
lpd-5
g
ROS production
MitoSox Fluorescence (AU)
3
2
1
0
****
****
con
nuo-5
lpd-5
h
Lipid oxidation
Absorbance C=O/ CH2
0.5
0.4
0.3
0.2
0.1
0.0
****
****
con
nuo-5
lpd-5
i
gst-4::GFP
Normalised GFP Intensity
3
2
1
0
****
**
con
nuo-5
lpd-5
j
hsp-6::GFP
Normalised GFP Intensity
15
10
5
0
****
****
con
nuo-5
lpd-5
k
dct-1::GFP
Normalised GFP Intensity
5
4
3
2
1
0
****
***
con
nuo-5
lpd-5
l
hlh-30::GFP
% Of animals wit nuclear localization of HLH-30::GFP
80
60
40
20
0
****
****
con
nuo-5
lpd-5

Figure 3

a

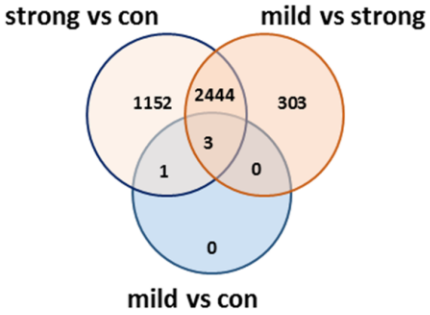

b

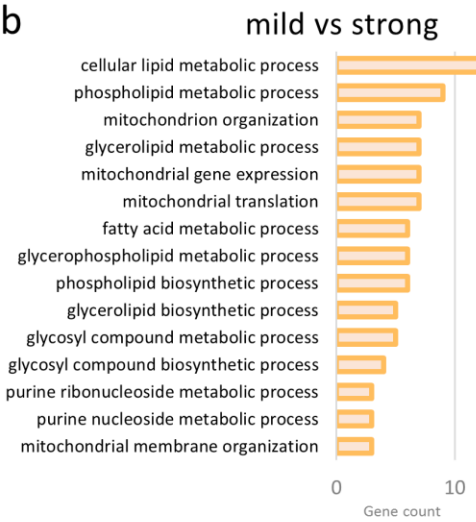

c

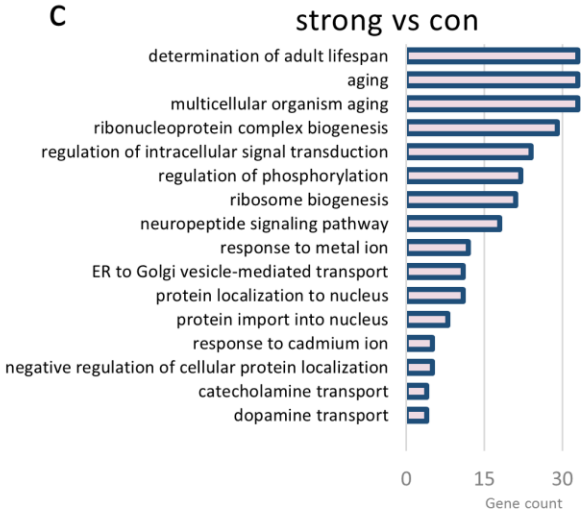

d

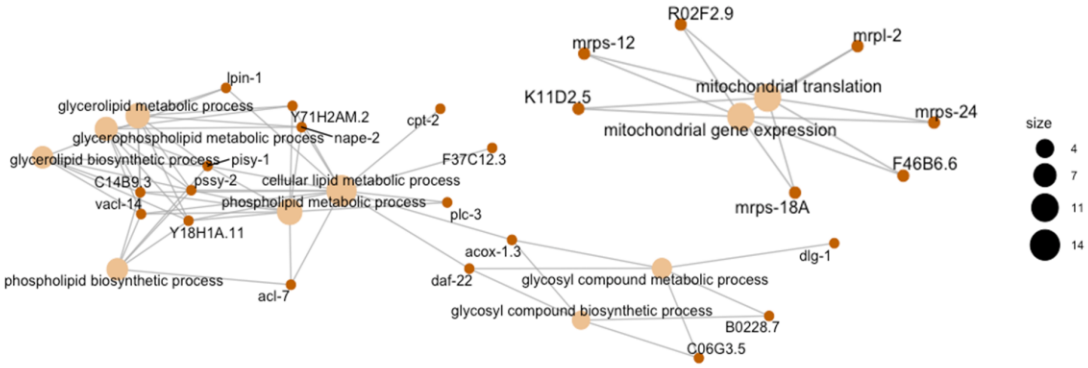

e

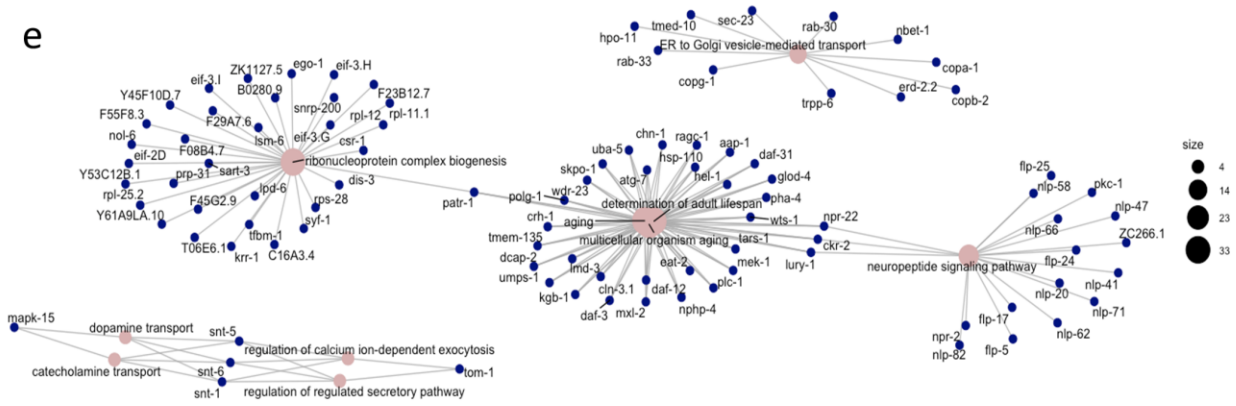

Figure 4

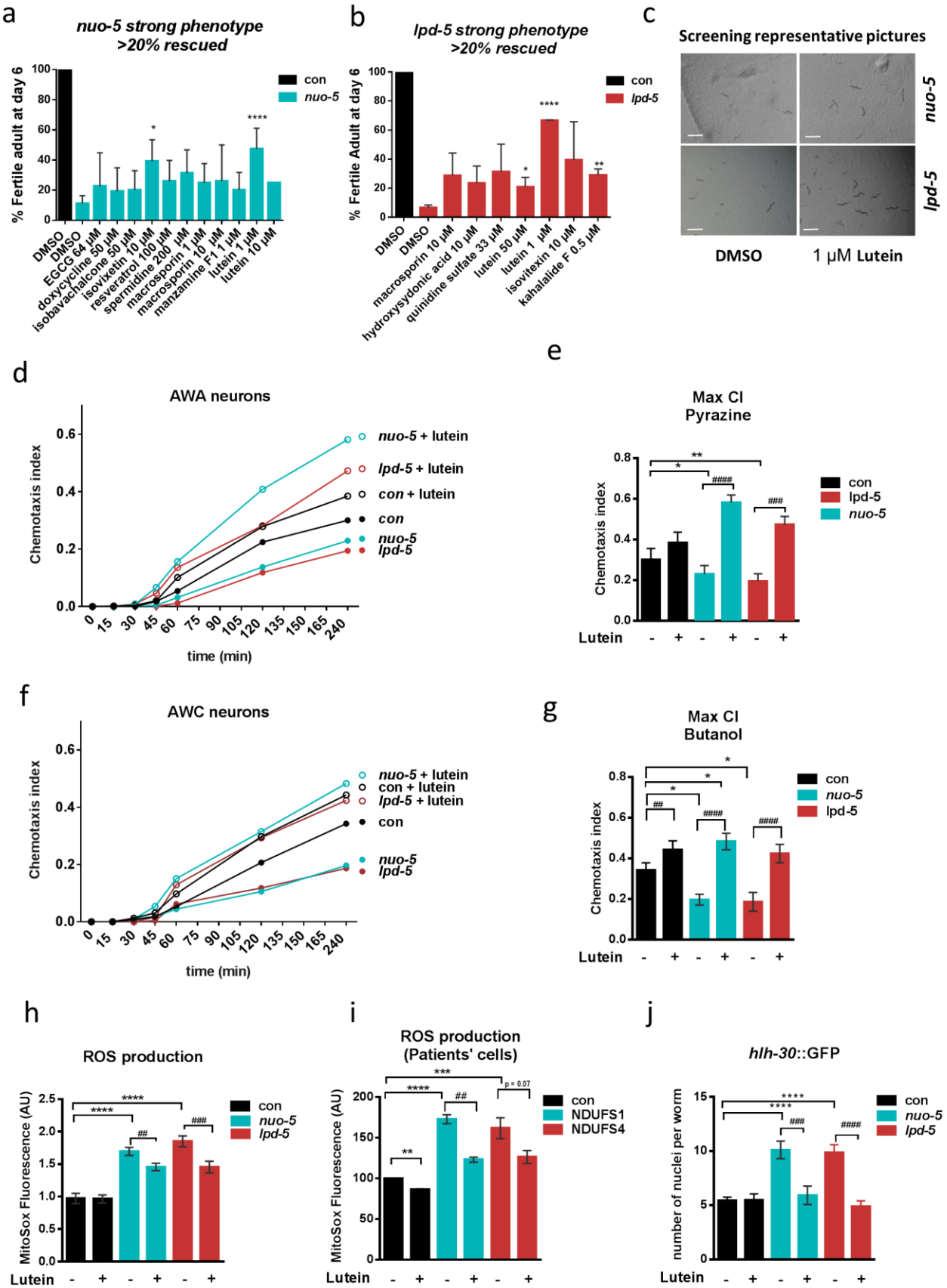
a
nuo-5 strong phenotype
>20% rescued
% Fertile adult at day 6
con
nuo-5
DMSO
DMSO
EGCG 64 µM
doxycycline 50 µM
isobavachalcone 50 µM
isovitexin 10 µM
resveratrol 100 µM
spermidine 200 µM
macrosporin 1 µM
macrosporin 10 µM
manzamine F1 1 µM
lutein 1 µM
lutein 10 µM
b
lpd-5 strong phenotype
>20% rescued
% Fertile Adult at day 6
con
lpd-5
DMSO
DMSO
macrosporin 10 µM
hydroxysydonic acid 10 µM
quinidine sulfate 33 µM
lutein 50 µM
lutein 1 µM
isovitexin 10 µM
kahalalide F 0.5 µM
c
Screening representative pictures
nuo-5
lpd-5
DMSO
1 µM Lutein
d
AWA neurons
Chemotaxis index
time (min)
nuo-5 + lutein
lpd-5 + lutein
con + lutein
con
nuo-5
lpd-5
e
Max CI
Pyrazine
Chemotaxis index
con
lpd-5
nuo-5
Lutein
f
AWC neurons
Chemotaxis index
time (min)
nuo-5 + lutein
con + lutein
lpd-5 + lutein
con
nuo-5
lpd-5
g
Max CI
Butanol
Chemotaxis index
con
nuo-5
lpd-5
Lutein
h
ROS production
MitoSox Fluorescence (AU)
con
nuo-5
lpd-5
Lutein
i
ROS production
(Patients' cells)
MitoSox Fluorescence (AU)
con
NDUFS1
NDUFS4
Lutein
j
hlh-30::GFP
number of nuclei per worm
con
nuo-5
lpd-5
Lutein

Figure 5

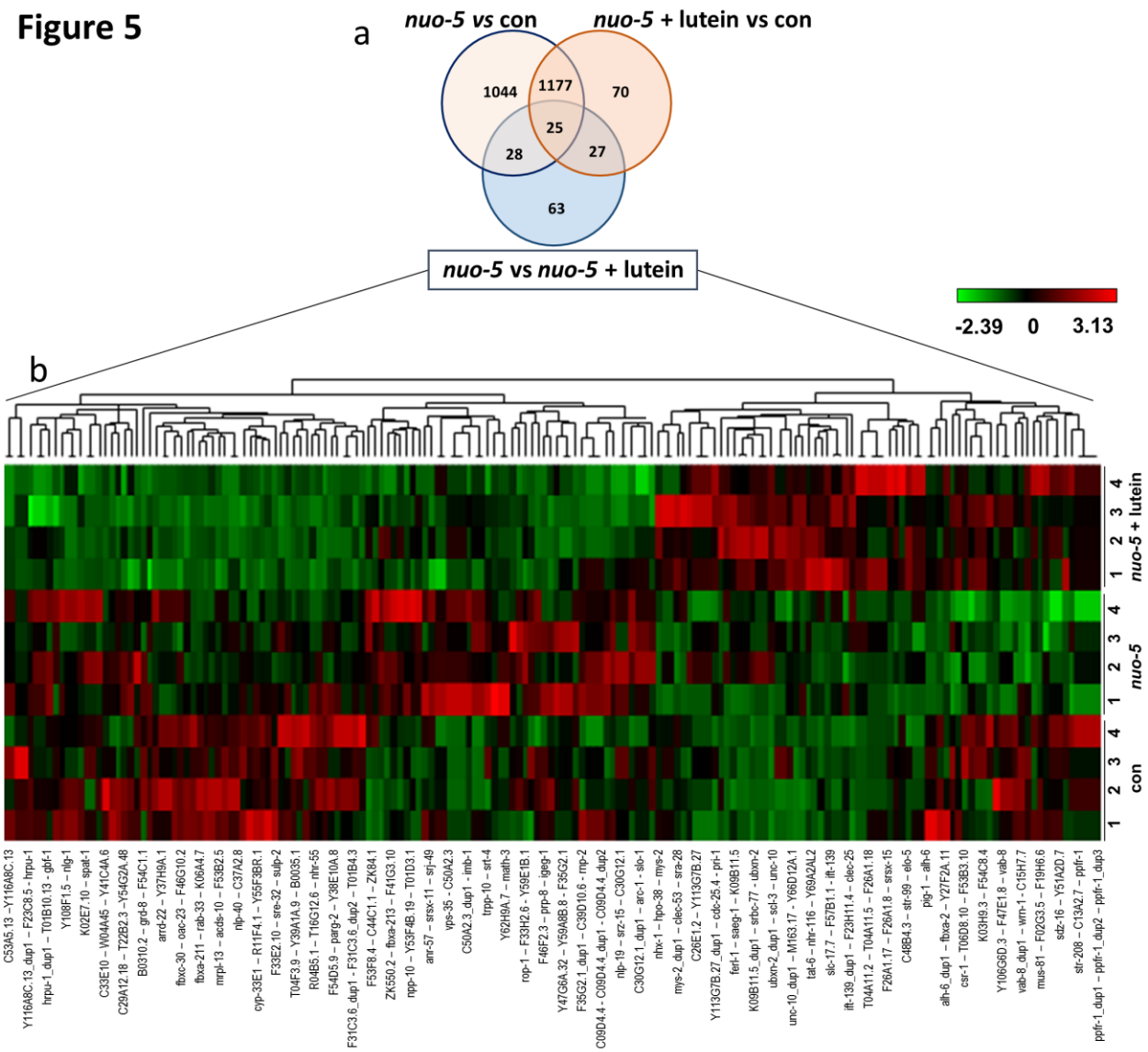
a
nuo-5 vs con
nuo-5 + lutein vs con
1044
1177
70
25
28
27
63
nuo-5 vs nuo-5 + lutein
-2.39
0
3.13
b
nuo-5 + lutein
nuo-5
con
1
2
3
4
C53A5.13 – Y116A8C.13
Y116A8C.13_dup1 – F23C8.5 - hrpu-1
hrpu-1_dup1 – T01B10.13 - gbf-1
Y108F1.5 – nlg-1
K02E7.10 – spat-1
C33E10 – W04A4.5 – Y41C4A.6
C29A12.18 – T22B2.3 –Y54G2A.48
B0310.2 – grd-8 – F54C1.1
arrd-22 – Y37H9A.1
fbxc-30 – oac-23 – F46G10.2
fbxa-211 – rab-33 – K06A4.7
mrpl-13 – acds-10 – F53B2.5
nlp-40 – C37A2.8
cyp-33E1 – R11F4.1 – Y55F3BR.1
F33E2.10 – sre-32 – sulp-2
T04F3.9 – Y39A1A.9 – B0035.1
R04B5.1 – T16G12.6 – nhr-55
F54D5.9 – parg-2 – Y39E10A.8
F31C3.6_dup1 - F31C3.6_dup2 – T01B4.3
F53F8.4 – C44C1.1 – ZK84.1
ZK550.2 – fbxa-213 – F41G3.10
npp-10 – Y53F4B.19 – T01D3.1
anr-57 – srsx-11 – srj-49
vps-35 - C50A2.3
C50A2.3_dup1 - imb-1
trpp-10 – srt-4
Y62H9A.7 – math-3
rop-1 – F33H2.6 - Y59E1B.1
F46F2.3 – prp-8 – igeg-1
Y47G6A.32 – Y59A8B.8 - F35G2.1
F35G2.1_dup1 – C39D10.6 - rnp-2
C09D4.4 - C09D4.4_dup1 - C09D4.4_dup2
nlp-19 – srz-15 – C30G12.1
C30G12.1_dup1 – arc-1 - slo-1
nhx-1 – hpo-38 – mys-2
mys-2_dup1 – clec-53 – sra-28
C26E1.2 – Y113G7B.27
Y113G7B.27_dup1 – cdc-25.4 - prt-1
ferl-1 – saeg-1 – K09B11.5
K09B11.5_dup1 – srbc-77 - ubxn-2
ubxn-2_dup1 – sci-3 – unc-10
unc-10_dup1 – M163.17 - Y66D12A.1
tat-6 – nhr-116 – Y69A2AL.2
slc-17.7 – F57B1.1 - ift-139
ift-139_dup1 – F23H11.4 – clec-25
T04A11.2 – T04A11.5 – F26A1.18
F26A1.17 – F26A1.8 – srsx-15
C48B4.3 – str-99 – elo-5
plg-1 – alh-6
alh-6_dup1 – fbxa-2 – Y27F2A.11
csr-1 – T06D8.10 – F53B3.10
K03H9.3 – F54C8.4
Y106G6D.3 – F47E1.8 – vab-8
vab-8_dup1 – wrn-1 - C15H7.7
mus-81 – F02G3.5 – F19H6.6
sdz-16 – Y51A2D.7
str-208 – C13A2.7 – ppfr-1
ppfr-1_dup1 – ppfr-1_dup2 – ppfr-1_dup3
c
nlp-40
regulation of secretion
Y69A2AL.2
secretion
modulation of chemical synaptic transmission
vps-35
endosomal transport
gbf-1
nlg-1
slo-1
neurotransmitter secretion
unc-10
signal release
signal release from synapse
regulation of trans-synaptic signaling
mitotic sister chromatid segregation
trpp-10
negative regulation of cell cycle process
csr-1
ppfr-1
sister chromatid segregation
nuclear transport
protein import
import into nucleus
mus-81
B0035.1
regulation of cell cycle phase transition
mitotic nuclear division
npp-10
F53B2.5
protein localization to nucleus
T16G12.6
imb-1
cell cycle phase transition
nucleocytoplasmic transport
protein import into nucleus
cdc-25.4

Figure 6

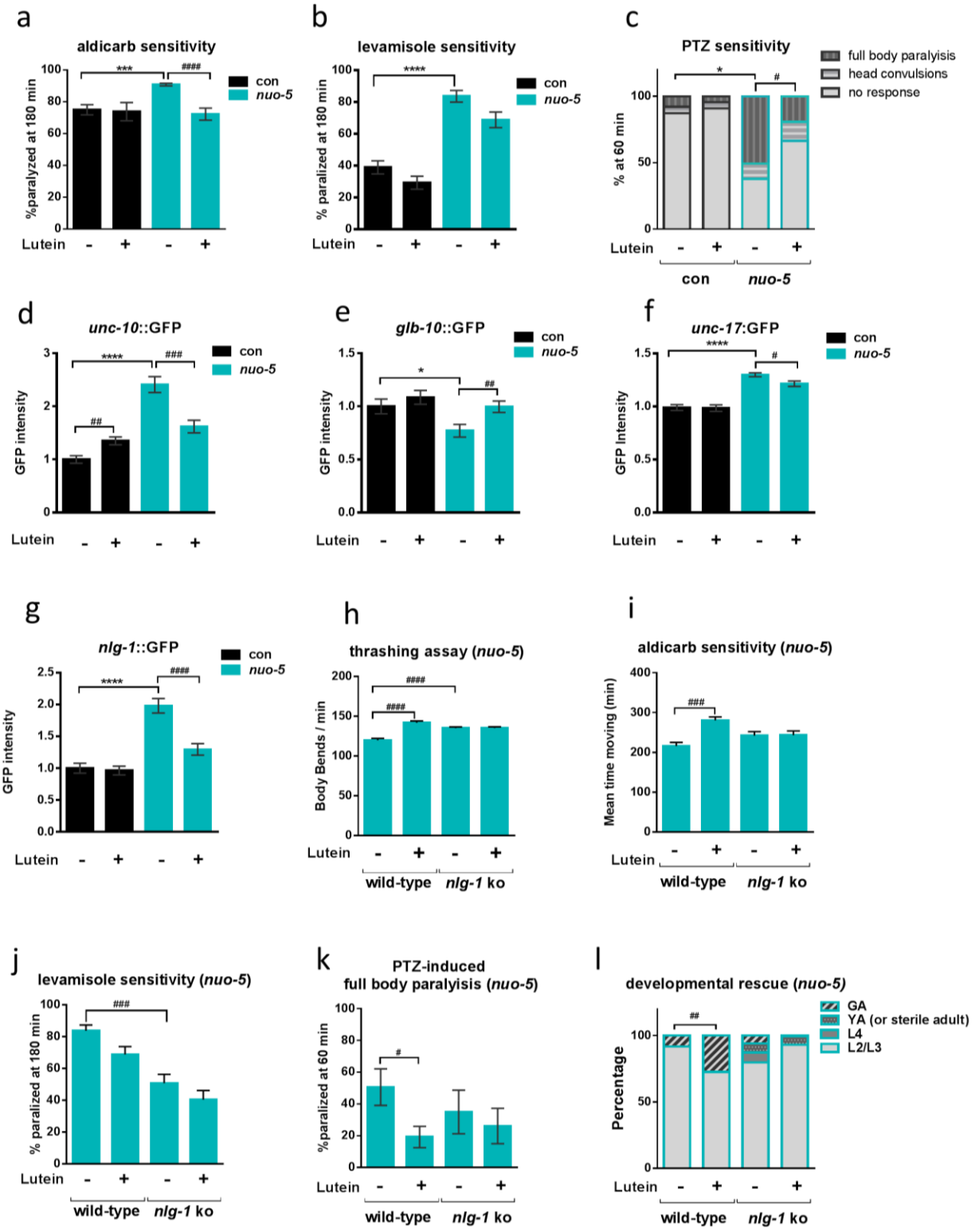
a
aldicarb sensitivity
%paralyzed at 180 min
con
nuo-5
Lutein
b
levamisole sensitivity
% paralized at 180 min
c
PTZ sensitivity
% at 60 min
full body paralyisis
head convulsions
no response
d
unc-10::GFP
GFP intensity
e
glb-10::GFP
f
unc-17:GFP
g
nlg-1::GFP
h
thrashing assay (nuo-5)
Body Bends / min
wild-type
nlg-1 ko
i
aldicarb sensitivity (nuo-5)
Mean time moving (min)
j
levamisole sensitivity (nuo-5)
k
PTZ-induced
full body paralyisis (nuo-5)
%paralized at 60 min
l
developmental rescue (nuo-5)
Percentage
GA
YA (or sterile adult)
L4
L2/L3

Figure 7

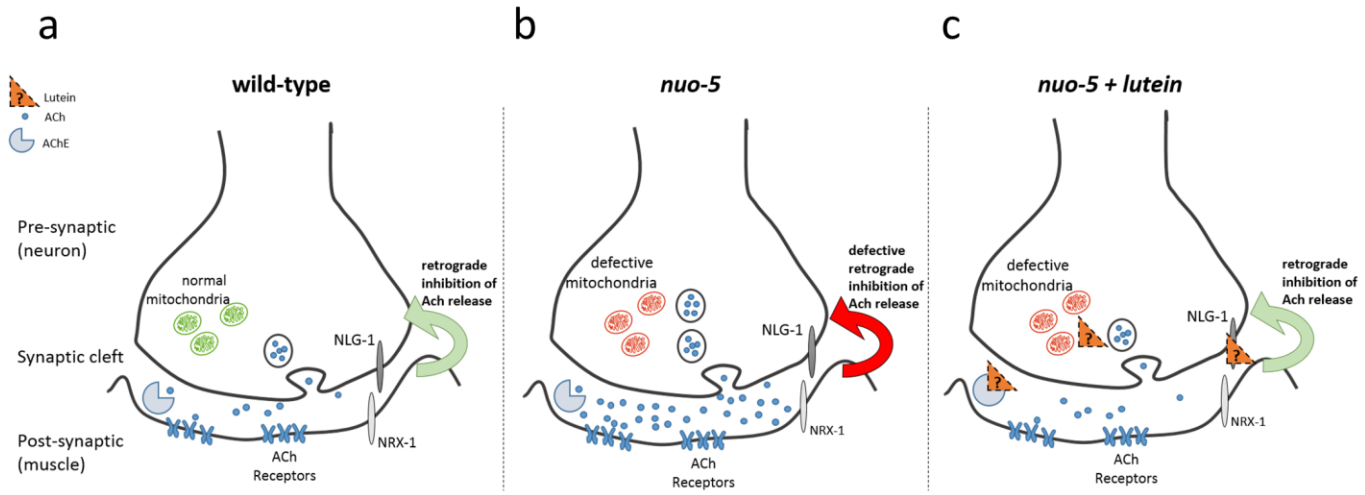

	wild-type	nuo-5	nuo-5 + lutein
Sensitivity to :			
- Aldicarb	normal	hypersensitive	rescued
- Levamisole	normal	hypersensitive	hypersensitive, partially rescued
- PTZ	normal	hypersensitive (full body paralysis)	rescued
Development :	normal	arrested	partially rescued
Thrashing in liquid :	normal	defective	rescued
Attraction to:			
- Pyrazine:	normal	defective	rescued
- Butanol:	normal	defective	rescued